Combination therapeutics of Niltotinib and radiation in Acute Lymphoblastic Leukemia as an effective method against drug resistance

A THESIS
SUBMITTED TO THE FACULTY OF THE GRADUATE SCHOOL
OF THE UNIVERSITY OF MINNESOTA
BY

Jackson Penning

IN PARTIAL FULFILLMENT OF THE REQUIREMENTS
FOR THE DEGREE OF
MASTER OF SCIENCE

Jasmine Foo, Ph.D.

August, 2016

Acknowledgements

Thank you to my adviser, Jasmine Foo, Ph.D., for guidance on this thesis as well as Kamran Kaveh, Ph.D., and Kevin Leder, Ph.D., with their collaboration on Chapter 1 of this thesis. Thank you also to our collaborator Susanta Hui, Ph.D. and his laboratory, who performed the experiments and provided the data.

Abstract

In this work we combine in vitro experimentation with mathematical modeling to study the combined effect of the tyrosine kinase inhibitor nilotinib and ionizing radiation on acute lymphoblastic leukemia cells. We develop a mathematical model for the cell response to this combined therapy. This mathematical model is parameterized via cell viability experiments conducted at a variety of different levels of nilotinib concentration and radiation exposure. We use this parameterized mathematical model to predict cell viability at new levels of nilotinib concentration. These predictions are then compared with new sets of cell viability experiments. We then investigate the structure of optimal radiation dosing schedules under our mathematical model. Finally, the model is expanded to incorporate an additional toxicity constraint on healthy lymphoblast cells, further characterizing optimized treatment protocols.

Contents

Acknowledgements i

Abstract ii

List of Tables v

List of Figures vi

1 Combination therapeutics of Nilotinib and radiation in Acute Lymphoblastic Leukemia as an effective method against drug resistance 1

1.1 Introduction 1

1.2 Materials and Methods 3

1.2.1 Experiment 3

1.2.2 Mathematical model 5

1.2.3 Dose-response functions 6

1.3 Results 8

1.3.1 In vitro viability experiments 8

1.3.2 Fitting to experimental data 9

1.3.3 Fractionated therapy and optimized radiation protocol 14

1.4 Discussion 15

2 Expansion and optimization of combination therapeutics of Nilotinib and radiation in Acute Lymphoblastic Leukemia 19

2.1 Introduction 19

2.2 Methods 20

2.2.1 Mathematical model 20
2.3 Results 23
2.3.1 Verification of the equilibrium of normal lymphoblasts 23
2.3.2 Efficacy of previously proposed therapy strategies to minimize tumor burden 27
2.3.3 Proposed therapy strategies with normal lymphoblast cell toxicity constraint 32
2.4 Discussion 38

3 References **44**

Appendices 46
A.1 Mutation-proliferation model 46
A.2 Continuous-time linear-quadratic formula 48

List of Tables

1.1 In vitro cell viability results, expressed as percentages, in response to Nilotinib, radiation, and combination therapy. All cultures had an initial viability of 93%. 8

1.2 Nilotinib dose-response coefficients for proliferation rates in control, drug-only and drug+radiation cases. (See Appendix A.2 for definition of $r_{0,1,2}$.) 11

1.3 Nilotinib dose-response coefficients for death rates in control, drug-only and drug+radiation cases. (See Appendix A.2 for definition of $d_{0,1,2}$.) . . 11

1.4 Model prediction for proliferation potentials of both sensitive and resistant cells for control, Nilotinibin-only and Nilotinib+radiation treatments. . 14

2.1 Optimal Dosing Strategies. The doses below are the output protocols determined with the opimization routine. *Comp* refers to direct competition model, *sep* is the separate population model, *C* is constant 18 nM nilotinib and *BL* is back-loaded nilotinib protocol. Each percentage is the minimum viability threshold for the given protocol. $d1, d2, d3, d4, d5$ are radiation fractions, with Gy units. 39

List of Figures

1.1 Treatment protocol used in the experiment. Acute radiation dose is administered at day 0 (IR). Doses of Nilotinib is administered every few days to keep the drug concentration in a constant level. (day 0,3,6,8,10). 3

1.2 The schematics of sensitive and resistant populations under radiation and/or TKI treatment. a) Soon after acute radiation treatment both cell populations drastically decrease but bounces back through repopulation. b) Upon Nilotinib treatment the sensitive population became disadvantaged and gradually the resistant population outgrow and total population grows back. It does not reach the original population size. c) Combining both therapies both populations are disadvantaged and treatment is much more effective. We have assumed a very small initial population of resistant cell before the treatment begins. 4

1.3 The cell viability versus time for ALL cell line after 2Gy (dash) and 4Gy (solid) irradiation (day 0). Solid lines show model predictions and circles are the in vitro experimental data. Thin lines show model results for varying radiosensitivity parameters by approximately ± 15 per cent. The values for parameters are reported in Table 1.4. $\alpha = 0.6647, \beta = 0.079$ and $\Delta\alpha = \pm 0.10, \Delta\beta = \pm 0.012$. 10

1.4 Evolution of Nilotinib resistance in ALL cell lines with and without radiation therapy in vitor (0-10 days). Lines are the model predictions and circles are experimental results. Red (dot dash) and magenta (long dash) correspond to 4Gy and 2Gy radiation without Nilotinib (control). With only Nilotinib treatment (18nM) after 6 days the resistant population is already grown (green, small dash plot). Combination of radiation (2 and 4 Gy) and Nilotinib significantly delays the evolution of resistance and improves the efficacy of the treatment (blue, dotted line: 2Gy + Nilotinib, cyan, solid line: 4Gy+Nilotinib). 12

1.5 LD_{50} assay for radiation dose-reponse. Solid lines are model predictions with parameters derived from our proposed Nilotinib dose-response function. (Model parameters are fixed from Fig.1.4) Cell viabilities are measured after three days. The dashed line (magenta) represents cell viabilities for zero drug concentration at various radiation doses and solid line (red) represent 18 nM Nilotinib at different radiation doses. 13

1.6 Model prediction of the Nilotinib dose-response function. The parameters in the model are fixed from other experiment (Fig. 1.4). We used the proposed Nilotinib dose-response combined with the dynamics of the system captured at day-3. The blue graph (solid line) depict results in the absence of radiation and matches very well with IC_{50} measurements. There are deviations for higher doses (25nM) which is not shown here. Other graphs present model predictions for efficacy of the treatment for various radiation doses of 1,2,3,and 4 Gy. 17

1.7 Comparison between four protocols: 5-fraction with 0.4Gy per fraction (blue, dot dash line), radiation optimal (black, dotted line), acute (green, solid line) and optimal radiation and adjusted Nilotinib (red, dashed line). Nilotinib concentration is 18 nM in the first three protocols, respectively, and increased over the 10 days of treatment in the latter protocol, averaging 18 nM per day. The total cell viability is clearly lowest for the optimal radiation at day 10 and beyond for the optimal radiation and Nilotinib dosing protocol. Only 4Gy gives nearly zero viability after 20 days. . . . 18

2.1 Normal cell equilibrium in the absence of treatment and tumor cells. Under spatial and resource constraints *in vitro*, the normal lymphoblast population has a steady state viability of around 90%. 24
2.2 Interaction of cell supbpopulations in the absence of treatment. Direct competition with resource constraints indicate lower and nearly equally viable subpopulations. Note, however, the severely diminished populations ($<$50%). 25
2.3 Subpopulations without treatment, with dynamics of *in vitro* growth separate between normal lymphoblast and tumor subpopulations. Note the slow transformation of Nilotinib sensitive to resistant cells while maintaining a steady state population equally viable to that of normal lymphoblasts. 26
2.4 Effect of optimization protocols previously determined on competitive subpopulations. The 2Gy acute with 18 nM Nilotinib (red, solid and dashed) and 5x0.4Gy fractions with 18 nM (green, dotted and dashed-dotted) are depicted. 28
2.5 Effect of optimization protocols previously determined on competitive subpopulations. The 2Gy optimal radiation protocol with constant 18 nM Nilotinib (magenta, solid and dashed lines) and optimal 2Gy radiation protocol with back-loaded Nilotinib (black, dotted and dashed-dotted lines) are depicted. 29
2.6 Effect of optimization protocols previously determined on separate subpopulations with separated subpopulations. The 2Gy acute with 18 nM Nilotinib (red, solid and dashed) and 5x0.4Gy fractions with 18 nM (green, dotted and dashed-dotted) are depicted. 30
2.7 Effect of optimization protocols previously determined on separate subpopulations. The 2Gy optimal radiation protocol with constant 18 nM Nilotinib (magenta, solid and dashed lines) and optimal 2Gy radiation protocol with back-loaded Nilotinib (black, dotted and dashed-dotted lines) are depicted. 31

2.8 Direct competition simulation with normal lymphoblast toxicity constraint greater than 60%, with constant nilotinib (18 nM). The surviving normal lymphoblasts after irradiation dominate the culture and out-compete the tumor cells. 33
2.9 Direct competition simulation with normal lymphoblast toxicity constraint greater than 60%, with back-loaded nilotinib protocol. The surviving normal lymphoblasts after irradiation dominate the culture and out-compete the tumor cells, with less radiation required. 34
2.10 Direct competition simulation with nilotinib-only protocol, constant 18 nM. Note the drop in normal lymphoblast viability below 70% secondary to competition with tumor cells. 35
2.11 Separate subpopulation simulation with constant 18 nM nilotinib and minimum threshold of 60% normal lymphoblasts. 36
2.12 Separate subpopulation simulation with back-loaded nilotinib and minimum threshold of 60% normal lymphoblasts. 37
2.13 Separate subpopulation simulation with constant 18 nM nilotinib and minimum threshold of 75% normal lymphoblasts. 38
2.14 Separate subpopulation simulation with back-loaded nilotinib and minimum threshold of 75% normal lymphoblasts. 39
2.15 Separate subpopulation simulation with constant 18 nM nilotinib and minimum threshold of 80% normal lymphoblasts. 40
2.16 Separate subpopulation simulation with back-loaded nilotinib and minimum threshold of 80% normal lymphoblasts. 41
2.17 Separate subpopulation simulation with constant 18 nM nilotinib and minimum threshold of 90% normal lymphoblasts. 42
2.18 Separate subpopulation simulation with back-loaded nilotinib and minimum threshold of 90% normal lymphoblasts. 43
1 A schematic of possible proliferation and death events and corresponding rates in our model. For brevity the effect of Nilotinib and radiation on death rates are shown. In principle Nilotinib affects division/proliferation rates as well. 47

Chapter 1

Combination therapeutics of Nilotinib and radiation in Acute Lymphoblastic Leukemia as an effective method against drug resistance

1.1 Introduction

Acute Lymphoblastic Leukaemia (ALL) is a disease of the blood system where immature lymphoblasts are overproduced. This overproduction of lymphoblasts can have two possible negative consequences: (1) the overly abundant lymphoblasts may invade and damage other organs, and (2) the production of normal fully functional blood cells may decline to a dangerously low level. There are several different genetic subtypes of ALL. One of the most prevalent, the Ph+ variant, is due to a translocation that results in the formation of the Philadelphia chromosome, which can be observed upon karyotyping. This translocation leads to the fusion of the abl tyrosine kinase gene with the bcr gene, leading to the BCR-ABL mutation. The protein product of this fusion

leads to uncontrolled cellular reproduction, and in the case of B cell acute lymphoblastic leukemia (B-ALL), this mutation fosters the transformation of immature B cells. This form of leukemia has a poor prognosis overall. A significant breakthrough in the treatment of Ph+ ALL (as well as the treatment of chronic myeloid leukemia [CML]) was the development of the tyrosine kinase inhibitor (TKI) Imatinib [10, 11]. This drug and the more potent second generation drugs Dasatinib and Nilotinib are able to selectively inhibit the BCR-ABL mutant protein and thus significantly reduce Ph+ cell counts [8, 12]. However, one of the challenges in treatment with these drugs is the development of chemoresistance to these tyrosine kinase inhibitors, including Nilotinib, resulting in the failure of the treatment [6, 4] (see also [13] and references therein).

While TKI therapy has long term efficacy in the treatment of CML, most ALL patients eventually relapse following treatment with TKI. Thus a common treatment protocol for ALL patients is TKI therapy until the first remission [9], after which, the patient has a stem cell transplantation. However, a stem cell transplantation is a potentially dangerous procedure. Thus, the ability to extend the efficacy of TKI therapy in Ph+ ALL patients has the potential to significantly improve patient outcomes. In this work, we investigate the potential of combining TKI therapy with radiation as a means of extending remission length in ALL patients. We pursue this goal by combining in vitro experimental work with a mathematical model. We experimentally investigate the in vitro response of ALL cells to therapy with the second line TKI, Nilotinib; radiotherapy; and radiotherapy plus Nilotinib. In these studies we see a clear benefit from the combination of radiotherapy and Nilotinib. In addition, we develop a mathematical model to aid in understanding how Nilotinib and radiotherapy interact. There has been previous work that has investigated combining TKI with alternative therapies in the treatment of Ph+ ALL. For example, it has been shown that Jak2 signaling is associated with bcr-abl [7]. In a Jak2 inhibitor AG490 was shown in vitro to decrease the viability of Nilotinib resistant cells in a dose-dependent fashion. More recently [2] investigated the combination of Nilotinib with MEK, AKT, and JNK inhibitors (individually combined with Nilotinib). They observed that the use of these inhibitors led to a greater reduction in cell viability, and furthermore less risk of Nilotinib resistance. In the current work we showed potential advantage of adding low dose radiation with chemotherapy to control tumor burden and developed a mathematical modeling to study the combined effects

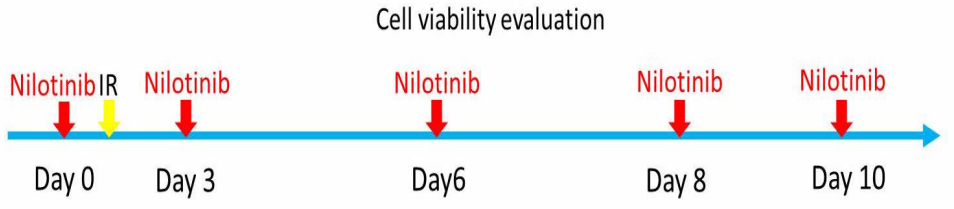

Figure 1.1: Treatment protocol used in the experiment. Acute radiation dose is administered at day 0 (IR). Doses of Nilotinib is administered every few days to keep the drug concentration in a constant level. (day 0,3,6,8,10).

of radiation and Nilotinib.

1.2 Materials and Methods

1.2.1 Experiment

1.2.1.1 Cell line

Bone marrow is harvested from an Arf-/- (p19-/-) mouse. Red blood cells are lysed and remaining cells are cultured overnight. Cells are then transduced with a retrovirus containing the BCR-ABL gene, which confers a leukemic phenotype. In that way, B cell acute lymphoblast leukemia cells were obtained and used in this study. Cells were maintained in alpha-MEM supplemented with 10% FBS, 20 mM L-glutamine, penicillin/streptomycin, and beta-mercapto-ethanol.

1.2.1.2 Treatment

For each culture, 5×10^5 cells were plated to each well of a 6-well plate, and the treatments were administered as shown in Figure 1. For the irradiation group, on day 0, cells were administered either 2 Gy or 4 Gy, by 225 kV X-ray beams using X-RAD 320 orthovoltage biological irradiator with a 0.35 mm copper filter. In the chemotherapy alone group, 18nM of Nilotinib was added in fresh media at days 0, 3, 6, and 8. We further investigated the combined effect of irradiation and chemotherapy. 18nM Nilotinib was added to the cells 4 hours before irradiation of 2Gy or 4Gy, followed by further administrations of Nilotinib in fresh media at days 3, 6, and 8. For all treatments, the

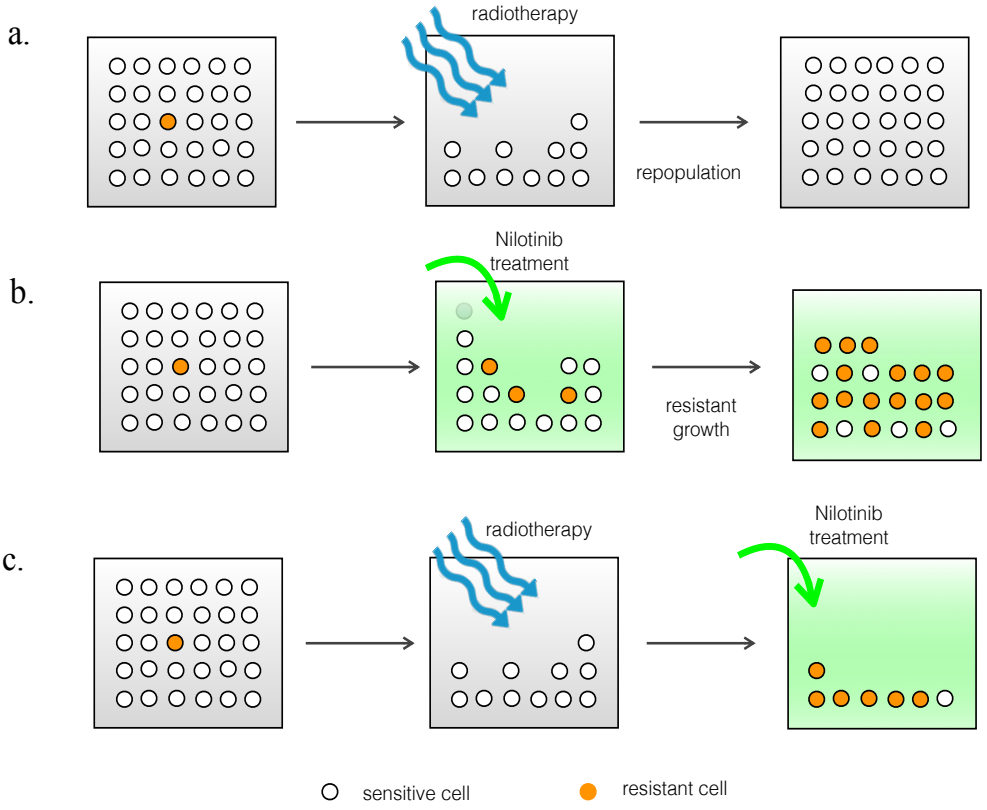

Figure 1.2: The schematics of sensitive and resistant populations under radiation and/or TKI treatment. a) Soon after acute radiation treatment both cell populations drastically decrease but bounces back through repopulation. b) Upon Nilotinib treatment the sensitive population became disadvantaged and gradually the resistant population outgrow and total population grows back. It does not reach the original population size. c) Combining both therapies both populations are disadvantaged and treatment is much more effective. We have assumed a very small initial population of resistant cell before the treatment begins.

cell culture medium was changed at days 0, 3, 6, and 8 to maintain the cells.

1.2.1.3 Cell viability assay

At days 1, 3, 6, 8 and 10, cell viability was assessed by the Trypan blue exclusion assay, and a hemocytometer was used to count the viable and dead cells. Viability was expressed as the percentage of viable cells of the total cell number. All measurements were done in triplicate.

1.2.2 Mathematical model

Our model is a coupled system of two ordinary differential equations. We consider two populations: a Nilotinib sensitive and a Nilotinib resistant population. Our differential equation model is a two-population logistic model with an additional term that allows conversion from Nilotinib sensitive to Nilotinib resistant phenotype in the presence of non-zero concentration of the drug.
Here we assume the following for the dynamics of the two subpopulations of the sensitive and resistant phenotypes:

- At the beginning of the experiment the majority of cells are Nilotinib sensitive. In the absence of the drug, the fitness of both phenotypes is considered to be the same.
- Both sensitive and resistant cells are resource constrained. In the presence of Nilotinib, resistant cells have a proliferative advantage over Nilotinib sensitive cells. Our model includes both a frequency-dependent division rate and a frequency-independent cell death term.
- In the presence of the drug sensitive cells mutate into resistant cells. This is due to the fact that random mutations among the sensitive population can give rise to a much more adaptive phenotype for high concentrations of Nilotinib. We assume this rate is constant. This is justified since the concentration of Nilotinib is kept constant during the experiment.

- The radiosensitivity of both phenotypes are set to be the same. The effect of Nilotinib on radiosensitivity is negligibly small. We also ignore any possible mutations that confer resistance due to ionizing radiation.

The mathematical model that describes the above mechanisms is detailed in Appendix A.1. We refer to this model as the proliferation-mutation model.

1.2.3 Dose-response functions

A key result in this work is identifying how Nilotinib, and Nilotinib plus radiation impact cell birth and death dynamics. We assume a linear dose response function that inhibition (of proliferation) and drug-induced apoptosis are both proportional to the concentration of the Nilotinib in the medium. Furthermore we assume that upon combining with radiotherapy the proportionality constant increases. This increase is also assumed to be proportional to the radiation dose. The above simple linear dose-response model can be written as follows:

$$\begin{aligned} (\text{proliferation rate}) &= r_0 - (\text{Nilotinib dose}) \times \big(r_1 + \text{radiation dose} \times r_2\big), \\ (\text{apoptosis rate}) &= d_0 + (\text{Nilotinib dose}) \times \big(d_1 + \text{radiation dose} \times d_2\big), \end{aligned} \tag{1.1}$$

where r_i's are constants that will need to be identified based on the experimental results. It is common to model dose response functions using a hill function structure (3- or 4-parameter logistic function). The hill function imposes a low level of drug efficacy at low doses and a saturation of drug efficacy at high doses. Since we are only modeling dose response at dosage levels near the IC-50 a linear model is sufficient. As will be seen in the next section, the results from this response function agrees with experiments for a wide range of low- and medium- doses. For high doses, as expected, there are some discrepancy between the mathematical model and observation.

We rewrite (1.1) in mathematical terms as

$$\begin{aligned} r_{\mathrm{S}} &= r_{\mathrm{S},0} - \big(r_{\mathrm{S},1} + r_{\mathrm{S},2}D\big)c, \\ r_{\mathrm{R}} &= r_{\mathrm{R},0} - \big(r_{\mathrm{R},1} + r_{\mathrm{R},2}D\big)c, \\ d_{\mathrm{S}} &= d_{\mathrm{S},0} + \big(d_{\mathrm{S},1} + d_{\mathrm{S},2}D\big)c, \\ d_{\mathrm{R}} &= d_{\mathrm{R},0} + \big(d_{\mathrm{R},1} + d_{\mathrm{R},2}D\big)c, \end{aligned} \tag{1.2}$$

where $r_{\mathrm{S,R}}$ denote the proliferation rates of sensitive and resistant populations. Similarly, $d_{\mathrm{S,R}}$ is the death rates of the two subpopulations. Coefficients r_i and d_i ($i \in \{0,1,2\}$) are the coefficients describing the dose response. Nilotinib dose is denoted by c. Values of r_0 and d_0 are the proliferation and death rates in the control case (Nilotinib-free medium). Coefficients r_1 and d_1 indicate how effective the treatment is (on each of the populations) and r_2 and d_2 determines the strength of radiation-drug interaction. Note that the signs are chosen so that Nilotinib decreases proliferation rates and decreases death rates for both sensitive and resistant cells. However these changes are expected to be more significant in sensitive cells. The effect of irradiation is to even further reduce proliferation and elevate death in both subpopulations.
It is also necessary to quantify the cell kill due to radiation. In particular, in the experimental results we noticed a significant drop in cell viability shortly after the application of ionizing radiation at dose rate of 1Gy/min on day zero. We quantify the effects of radiation cell kill with the standard linear quadratic model

$$\text{Surviving fraction} = \exp\big(-\alpha \times \text{radiation dose} - \beta \times (\text{radiation dose})^2\big)$$

where α and β are the radio-sensitivity parameters to be determined from the experimental data. In short, α represents the rate of cell kill due to single tracks of radiation and β represents cell kill due to two independent radiation tracks. The linear quadratic model is widely used due to its excellent agreement with empirical data for a wide range of radiation doses [5]. Values of α and β depends on the cell lines used in the experiment and sometimes the medium or microenvironmental factors. In Appendix A.2 we explain how to incorporate the linear quadratic framework for surviving fraction into our mutation-proliferation model (an ODE model).

Treatment	Day 1	Day 3	Day 6	Day 8	Day 10
control	96.2	94.1	90.6	89.7	91.3
18nM Nilotinib	85.2	58.5	57.2	67.3	68.3
2 Gy Radiation	31.9	50.3	83.3	85.2	87.8
18nM Nilotinib + 2 Gy Radiation	15.7	9.1	6.8	5.8	9.9
4 Gy Radiation	10.4	12.3	39.5	87.3	83.1
18nM Nilotinib + 4 Gy Radiation	4.1	4.9	1.0	0.6	0

Table 1.1: In vitro cell viability results, expressed as percentages, in response to Nilotinib, radiation, and combination therapy. All cultures had an initial viability of 93%.

1.3 Results

1.3.1 In vitro viability experiments

We evaluated the cell viability of the BCR-ABL cells in vitro in response to Nilotinib, radiation, or combination therapy with both Nilotinib and radiation. Radiation alone had an LD50 of 2 Gy. In response to radiation alone, there was an initial large reduction in viability attributed to the cell killing by radiation. Yet the cells were able to recover and repopulate rapidly, reaching 80% viability by day 6 for 2 Gy and day 8 for 4 Gy. Nilotinib alone, with an IC50 of 18nM, when administered constantly, and showed an incremental reduction in cell viability over the first 6 days, to about 57.2%, after which the cells began to develop a resistance to the drug and viabilities began to increase. When used in combination, Nilotinib + radiation appeared to have a more dramatic cell killing, and maintained the low levels of viable cells. In both radiation doses, the initial reduction in viability was further reduced by the additional treatment with Nilotinib. After this reduction, the cell viabilities maintained very low numbers, under 10% for the duration of the experiment. There was nearly no recovery of the cells, and nearly no resistance to Nilotinib observed, with the Nilotinib + 4 Gy cell population being entirely eliminated. Thus, the combination therapies were able to not only kill the cells, but also to maintain control of low cell viabilities over a longer time period.

1.3.2 Fitting to experimental data

We fit the model parameters using cell viability data with or without Nilotinib and in three radiation doses (0,2,4 Gy). We first estimate the the parameters $r_{\mathrm{S},0}$, $d_{\mathrm{S},0}$, K, α and β by fitting the mutation-proliferation model to cell viability data time series data in the absence of Nilotinib. This parameter estimation is carried out by minimizing mean square distance of model prediction to the observed data over all feasible parameter values. This minimization is carried out using an optimization routine within the software MATLAB. The parameter estimates obtained by this process were $\alpha = 0.6647$, $\beta = 0.0794$, $r_{\mathrm{S},0} = r_{\mathrm{R},0} = 2.5369$, and $d_{\mathrm{S},0} = d_{\mathrm{R},0} = 2.0550$. In Figure 1.3 we plot the model predictions for this parameter set and compare with the experimental data. In addition we include plots of model predictions for larger and smaller values of α and β. An alternative analytical derivation of radio-sensitivities can be performed from the LD50 assays which is discussed in Appendix A.2. The cell viabilities at day 1 for 0.5Gy radiation dose (from fractionated therapy results) and 2Gy are equated with analytical solution of the model in this case.

Next we fit model parameters in the absence of irradiation and in the presence of Nilotinib. Using the numerical solutions of the proliferation-mutation model optimized for the experimental data points we can determine the coefficients linear in the Nilotinib dose-response function (r_1 and d_1). The optimized coefficients are $r_{1,\mathrm{S}} = 0.0159, r_{1,R} = 0.0, d_{1,\mathrm{S}} = 0.0, d_{1,\mathrm{R}} = 0.0$. Also, the transformation rate is $\nu = 0.0409$. The above values translate into total proliferation and death rates of two populations as $r_{\mathrm{S}} = 2.2507, r_{\mathrm{R}} = 2.5369, d_{\mathrm{S}} = d_{\mathrm{R}} = 2.0550$. This indicates an increase in fitness of resistant cells relative to sensitive cells. Total fitness of sensitive cells $f_{\mathrm{S}} \equiv r_{\mathrm{S}} - d_{\mathrm{S}} = 0.1957$ while $f_{\mathrm{R}} \equiv r_{\mathrm{R}} - d_{\mathrm{R}} = 0.4819$. Using various initial population sizes of resistant cells in our model we confirmed that small existing initial population of resistant cells, or lack of it, does not change the model parameter as much. For consistency we used initial population of resistant cells as 0.001 and sensitive cells as 0.999 fraction of the total population.

The combination therapy with radiation and drug is preformed for two radiation doses (2, 4 Gy) and one drug does (18 nM). We used same fitting methods to find best fit parameters for the model using 2Gy + Nilotinib case. The parameters $r_{2,\mathrm{S}} = 0.0140, r_{2,\mathrm{R}} = 0.0, d_{2,\mathrm{S}} = 0.0025, d_{2,\mathrm{R}} = 0.0114$. These results are indicative that the

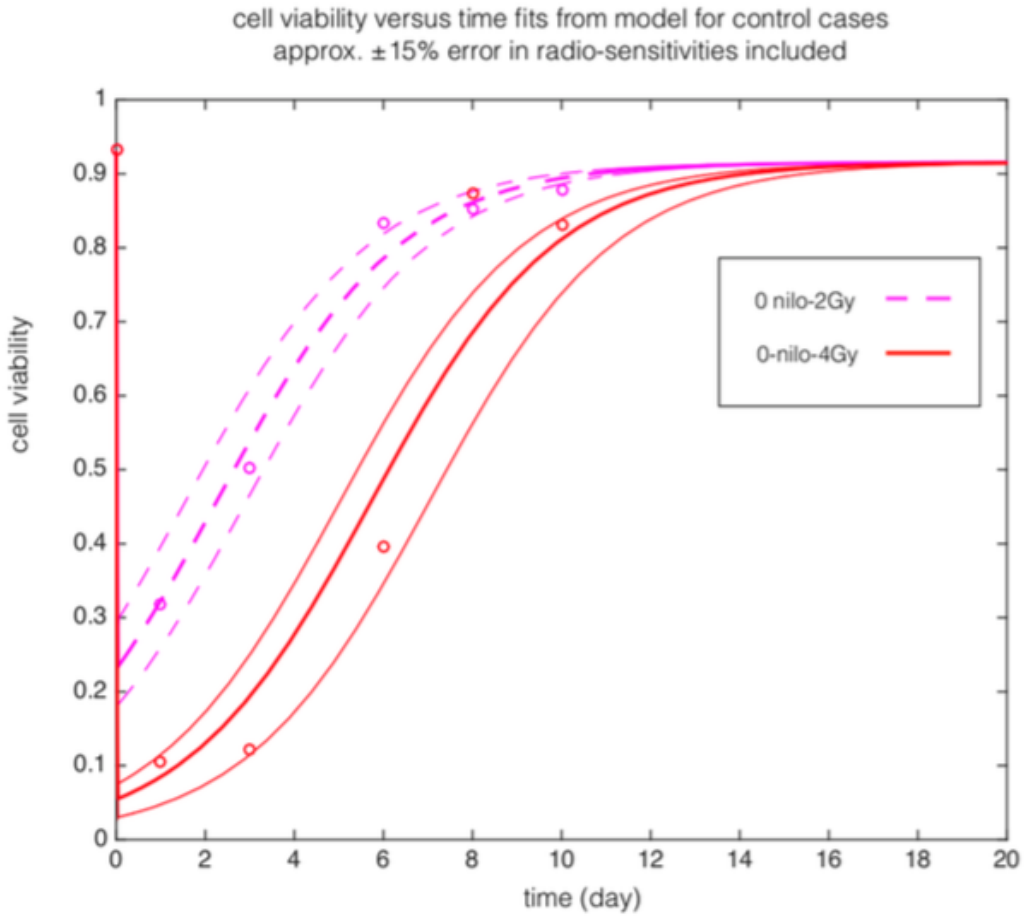

Figure 1.3: The cell viability versus time for ALL cell line after 2Gy (dash) and 4Gy (solid) irradiation (day 0). Solid lines show model predictions and circles are the in vitro experimental data. Thin lines show model results for varying radiosensitivity parameters by approximately ± 15 per cent. The values for parameters are reported in Table 1.4. $\alpha = 0.6647, \beta = 0.079$ and $\Delta\alpha = \pm 0.10, \Delta\beta = \pm 0.012$.

	$r_{0,\mathrm{S}}$	$r_{0,\mathrm{R}}$	$r_{1,\mathrm{S}}$	$r_{1,\mathrm{R}}$	$r_{2,\mathrm{S}}$	$r_{2,\mathrm{R}}$
control	2.5369	2.5369	0.0	0.0	0.0	0.0
nilo-only	2.5369	2.5369	0.0155	0.0	0.0	0.0
nilo+rad	2.5369	2.5369	0.0155	0.0	0.0140	0.0

Table 1.2: Nilotinib dose-response coefficients for proliferation rates in control, drug-only and drug+radiation cases. (See Appendix A.2 for definition of $r_{0,1,2}$.)

	$d_{0,\mathrm{S}}$	$d_{0,\mathrm{R}}$	$d_{1,\mathrm{S}}$	$d_{1,\mathrm{R}}$	$d_{2,\mathrm{S}}$	$d_{2,\mathrm{R}}$
control	2.0550	2.0550	0.0	0.0	0.0	0.0
nilo-only	2.0550	2.0550	0.0	0.0	0.0	0.0
nilo+rad	2.0550	2.0550	0.0	0.0	0.0025	0.0114

Table 1.3: Nilotinib dose-response coefficients for death rates in control, drug-only and drug+radiation cases. (See Appendix A.2 for definition of $d_{0,1,2}$.)

radiation tyrosine-kinase inhibitor interaction is most observed in the resistant population. This is not surprising as in the presence of Nilotinib the sensitive population is already highly disadvantaged. The transformation rate ν in this case is independent of radiation dose and estimated $\nu = 0.1768$. This is higher than the Nilotinib-only value for mutation/transformation rate, $\nu = 0.0409$. The above results are plotted in Fig. 1.4. Notice that all the above coefficients are the same for 2Gy +Nilotinib and 4Gy+Nilotinib cases. The good fit of the model is a sign that the proposed radiation-drug interaction term in the linear dose-response is a good approximation. All the above results are summarized in the Table 1.2 and Table 1.3. The proliferation potentials of both phenotypes and transformation rates are summarized in Table 1.4.

We can now check the consistency of the above model with all the parameters fixed with the IC_{50} and LD_{50} measurement assays for the same cell lines. The model prediction versus the experimental results for 0 and 18 nM Nilotinib for various radiation doses are plotted in Fig. 1.5. As can be seen the results are in very good agreement. Notice that the results are in fact model predictions and all the model parameters are fixed from previous experiments. The IC_{50} measurement assay results are done for 0 Gy only. The model prediction matches very well with these results as shown in Fig 1.6. Also plotted are cell viabilities for various radiation doses using the dose-response function for 1,2,3 and 4 Gy. The results are further plotted for 0-22nM of Nilotinib. In higher doses there is discrepancy with experiment (25nM 0Gy).

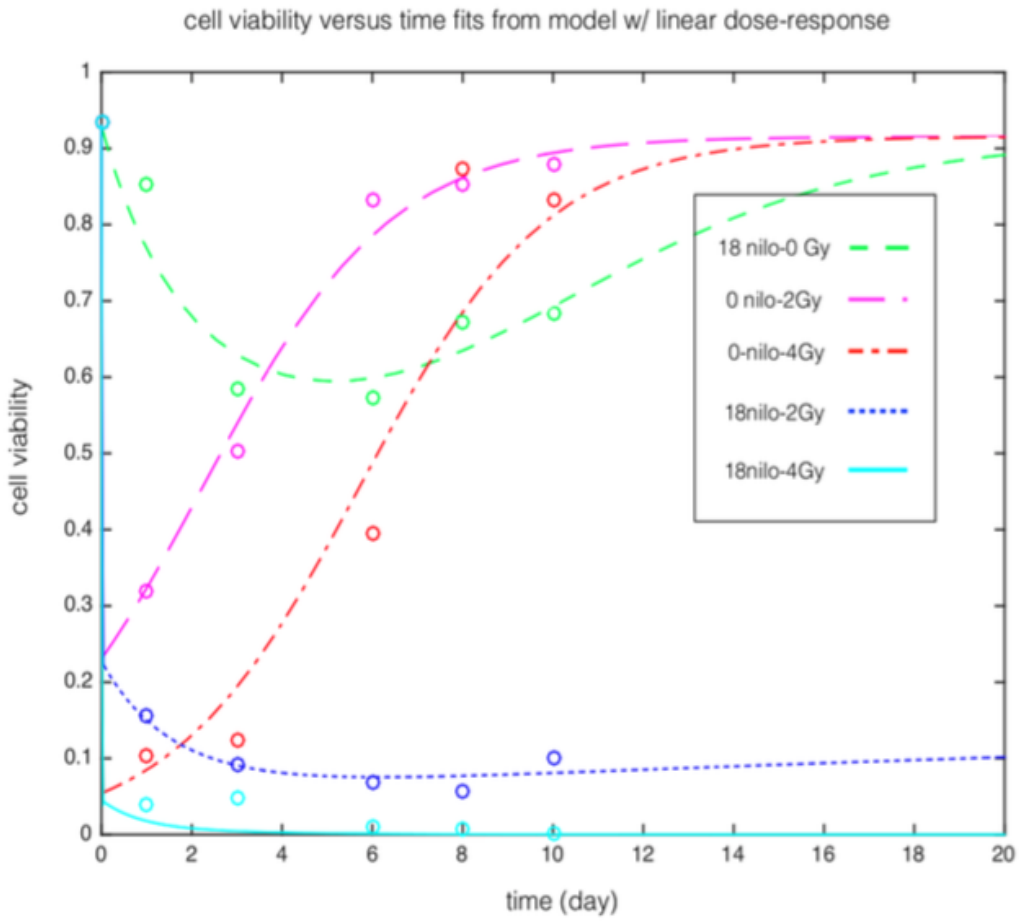

Figure 1.4: Evolution of Nilotinib resistance in ALL cell lines with and without radiation therapy in vitor (0-10 days). Lines are the model predictions and circles are experimental results. Red (dot dash) and magenta (long dash) correspond to 4Gy and 2Gy radiation without Nilotinib (control). With only Nilotinib treatment (18nM) after 6 days the resistant population is already grown (green, small dash plot). Combination of radiation (2 and 4 Gy) and Nilotinib significantly delays the evolution of resistance and improves the efficacy of the treatment (blue, dotted line: 2Gy + Nilotinib, cyan, solid line: 4Gy+Nilotinib).

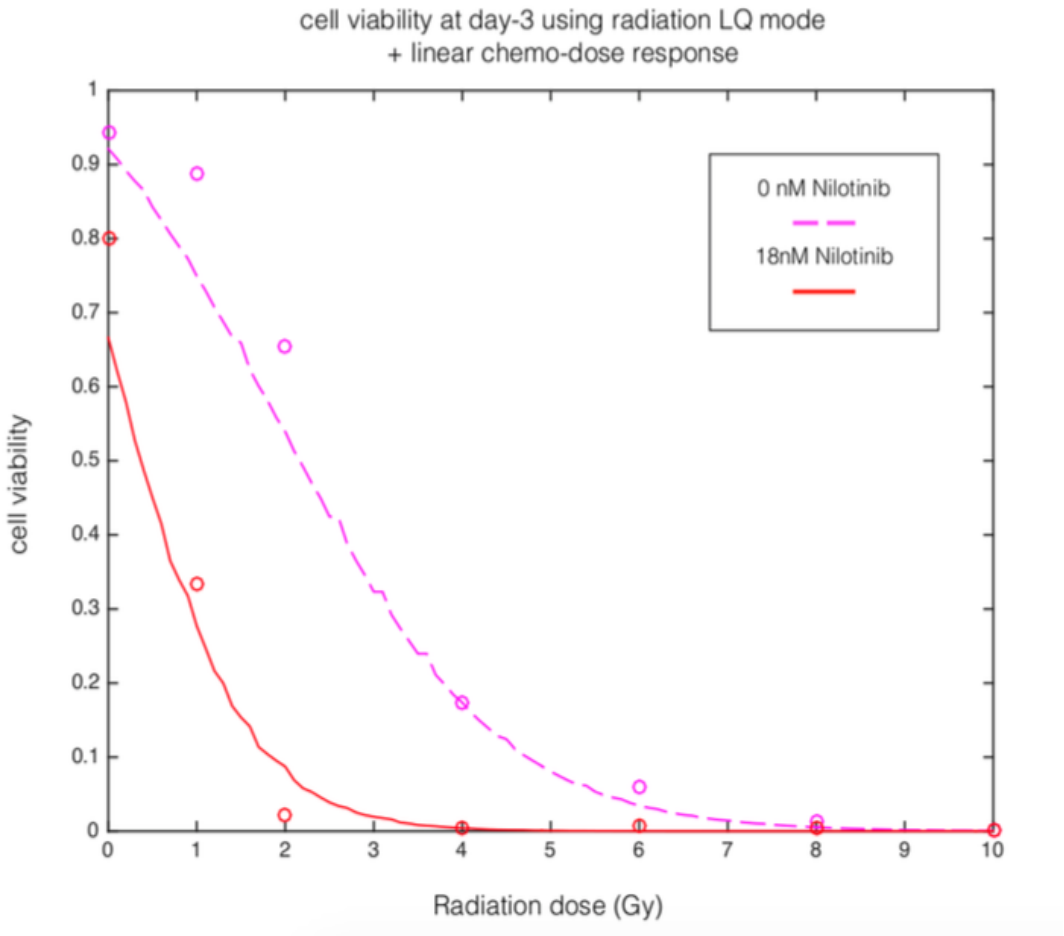

Figure 1.5: LD_{50} assay for radiation dose-reponse. Solid lines are model predictions with parameters derived from our proposed Nilotinib dose-response function. (Model parameters are fixed from Fig.1.4) Cell viabilities are measured after three days. The dashed line (magenta) represents cell viabilities for zero drug concentration at various radiation doses and solid line (red) represent 18 nM Nilotinib at different radiation doses.

	r_{S}	r_{R}	d_{S}	d_{R}	ν
control	2.5369	2.5369	2.0550	2.0550	0.0
nilo-only	2.2579	2.5369	2.0550	2.0550	0.0409
nilo+ 2Gy	1.7539	2.5369	2.1450	2.4654	0.1768
nilo+ 4Gy	1.2499	2.5369	2.2350	2.8758	0.1768

Table 1.4: Model prediction for proliferation potentials of both sensitive and resistant cells for control, Nilotinibin-only and Nilotinib+radiation treatments.

1.3.3 Fractionated therapy and optimized radiation protocol

We next use the computational model to identify potential combination strategies. We first assume the patient has been given a standard constant dose of Nilotinib (18 nM) and begin to explore various radiation fractionation protocols to be given in combination with the TKI. We considered a five-day radiation where the totaled summed dose is constant. The total dose is set to 2Gy as an example, within reasonable dosing limits for the experiment. We seek to minimize the total number of ALL cells at day 10. The control parameters are the radiation doses at days $0, 1, 2, 3$ and 4 which we denote with $d_i (i = 1, 2, 3, 4, 5)$. The optimal schedule is given by: $d_1 = 0.9371, d_2 = 0.5139, d_3 = 0.6445, d_4 = 0.0450, d_5 = 0.0064$. This front-loads the radiation on the first 3 days. In between each two radiation dose fractions, both cell types undergo repopulation. For acute radiation protocols, the linear dose response function predicts a change in proliferation potentials of both resistant and sensitive cells which depends on the total radiation dose (at day 0). For a fractionated protocol, we assume that the proliferation potentials of two cell types between the kth and $k + 1$th radiation doses depends on total radiation dose administered $until$ fraction k. The model prediction for total cell viabilities versus time for the optimal fractionation protocol is plotted in Fig. 1.3.3 and compared with a constant 5-fraction protocol ($d_i = 0.4$) and acute radiation treatment ($d_1 = 2, d_{2,3,4,5} = 0.0$). As can be seen at larger times the optimal protocol is clearly the most effective among the three cases considered.

The computational model can then be expanded to consider various dosing strategies of Nilotinib in an attempt again to minimize the ALL cell population at day 10. Concurrent use of the 5-day front-loaded radiation therapy with a new Nilotinib delivery

strategy over 10 days proves to be a more successful therapeutic approach. This alternate Nilotinib delivery strategy maintains the average daily dose to be 18 nM, however begins at a lower concentration and increases throughout the therapy duration, given by three days of 10 nM, followed by four days of 18 nM, and finally three days of 26 nM Nilotinib. The Nilotinib dose returns to 18 nM for the duration of the simulation after that time. Essentially, we are back-loading the chemotherapy dose onto the irradiated ALL cells. This may be visualized in Fig 1.3.3 as well, where at larger times the new strategy of Nilotinib dosing further reduces the ALL tumor burden.

1.4 Discussion

In this work we investigated the possible interaction between radiation therapy and tyrosine kinase inhibitor drug treatment, Nilotinib, in acute lymphoblastic leukemia using in vitro experimentation data. As the in vitro result shows, a day-0 radiation therapy before a longer term TKI treatment increases both the efficacy the treatment as well as prohibiting or delaying the development of resistance to Nilotinib. Even though the experiment is performed on ALL cell lines with Nilotinib treatment, we believe this positive radiation-drug interaction is a more general feature and might be observed in other forms of leukemia as well. Further, we constructed a dynamical model to explain the observations and predict response to various radiation and drug doses. The model assumes two populations of drug-sensitive and drug-resistant cells and uses a Nilotinib dose-response function that determines the proliferation strength of both populations. In this, we assume a linear regression model for dose-response function, as well as a transformation rate from a drug sensitive cell to drug resistant cell. We show that initial population of resistant phenotype is not important and model the radiation induced apoptosis by a continuous-time linear-quadratic model. The functional form of dose-response function after fitting with cell viability versus time experiments for various radiation and drug does combinations was fixed. The response function incorporates interaction between radiation an drug dose as well, which means that the elevation in drug induced apoptosis or depletion of resistant and sensitive cell proliferation is proportional to both drug dose times radiation dose. Our model and the dose-response function we proposed can predict total cell viability as a function of both radiation and

drug dose at various time points. More importantly, our model can assist the prediction of the time to acquire resistance for each combination of drug and radiation doses.

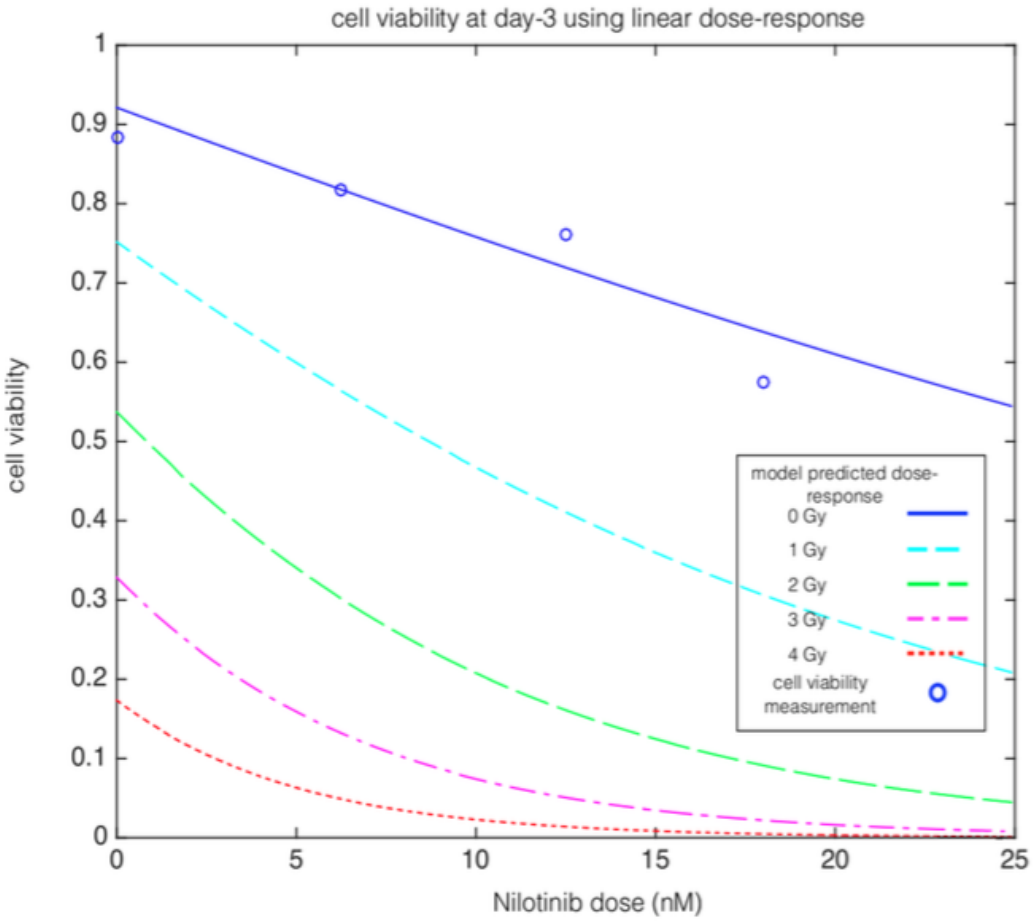

Figure 1.6: Model prediction of the Nilotinib dose-response function. The parameters in the model are fixed from other experiment (Fig. 1.4). We used the proposed Nilotinib dose-response combined with the dynamics of the system captured at day-3. The blue graph (solid line) depict results in the absence of radiation and matches very well with IC_{50} measurements. There are deviations for higher doses (25nM) which is not shown here. Other graphs present model predictions for efficacy of the treatment for various radiation doses of 1,2,3,and 4 Gy.

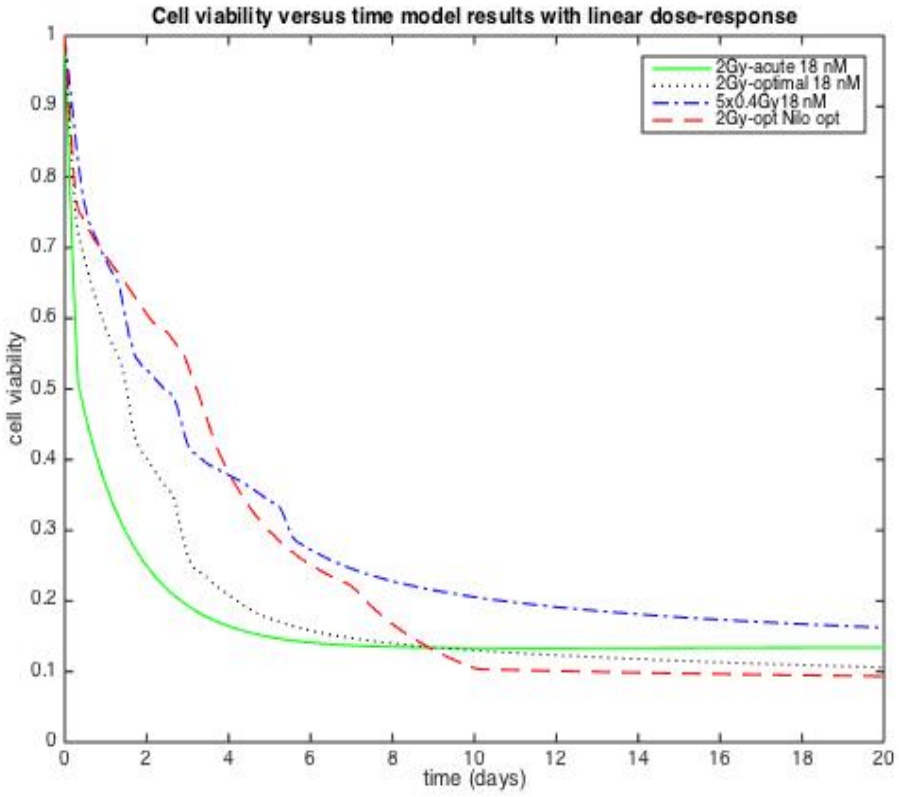

Figure 1.7: Comparison between four protocols: 5-fraction with 0.4Gy per fraction (blue, dot dash line), radiation optimal (black, dotted line), acute (green, solid line) and optimal radiation and adjusted Nilotinib (red, dashed line). Nilotinib concentration is 18 nM in the first three protocols, respectively, and increased over the 10 days of treatment in the latter protocol, averaging 18 nM per day. The total cell viability is clearly lowest for the optimal radiation at day 10 and beyond for the optimal radiation and Nilotinib dosing protocol. Only 4Gy gives nearly zero viability after 20 days.

Chapter 2

Expansion and optimization of combination therapeutics of Nilotinib and radiation in Acute Lymphoblastic Leukemia

2.1 Introduction

Acute lymphoblastic leukemia is a disease of the blood system in which immature lymphoblasts are overproduced. This overproduction of lymphoblasts can have two possible negative consequences: (1) the overly abundant lymphoblasts may invade and damage other organs, and (2) the production of normal fully functional blood cells may decline to a dangerously low level. There are various genetic subtypes of leukemia, and one of the most prevalent is that of the translocation mutation of the BCR and ABL proteins, commonly referred to as the Philadelphia chromosome (denoted Ph+). Previous work has investigated the combination therapeutics of concurrent chemotherapy, Nilotinib, and radiation therapy. This modeling has shown that the concurrent use of both therapies provides greatest benefit in the long run in terms of tumor suppression. A common feature of chemotherapies is inevitable drug resistance that arises from prolonged treatment with a specific drug (see sources in Chapter 1). This is known

to occur in Ph+ cells, specifically a point mutation in the binding site for nilotinib. The targeted concurrent therapy with radiation greatly reduces the tumor population in previous results, performed *in vitro*. An improved combination therapy course is thus less likely to produce drug resistant strains of the tumor, and improve survivability.

These *in vitro* experiments performed included only tumor populations. Current clinical practice of both radiation and chemotherapy must take into account the effect these therapies have on normal cells of the body. Thus, radiation treatments and chemotherapy regimens must be calibrated so as to minimize side effects, that is, maximize normal cell survivability, as well as minimize tumor burden. A natural extension of the model discussed in Chapter 1 is to include normal lymphoblastic blood cells in the experimentation with the tumor cells and predict the possible effect the concurrent treatment will have on the normal cells. This prediction will allow for optimization strategies for combination therapies specific for ALL.

In this work we will thus investigate the introduction of a normal lymphoblast cell line into the model previously proposed for ALL response to concurrent therapy to investigate the dual effect of the therapy on the normal cell population and tumor suppression. A theoretical model will be proposed and validated, and then will extend to include results from the aforementioned study to further optimize a treatment protocol for ALL. This expanded model lends to a more realistic biological and clinically relevant mathematical model.

2.2 Methods

2.2.1 Mathematical model

The model is a system of three ordinary differential equations representing three populations: a normal lymphoblast population, and Nilotinib sensitive and Nilotinib resistant tumor subpopulations. Logistic terms impose resource limitation on each population. There is an additional term that allows the conversion from Nilotinib sensitive to Nilotinib resistant phenotype in the precent of non-zero concentration of the drug.

More specifically, we assume the following for the dynamics of the two tumor subpopulations of sensitive and resistant phenotypes:

- At the beginning of the experiment the majority of cells are Nilotinib sensitive. In the absence of the drug, the fitness of both phenotypes is considered to be the same.

- Both sensitive and resistant cells are resource constrained, with the presence of normal lymphoblasts. In the presence of Nilotinib, resistant cells have a proliferative advantage over Nilotinib sensitive cells. Our model includes both a viability-dependent division rate and a viability-independent cell death term. Further, the physiology of the tumor subpopulations dictates that the tumor phenotype has a greater proliferation rate over normal lymphoblasts.

- In the presence of Nilotinib sensitive cells can mutate at a constant rate into resistant cells. This is due to the fact that random mutations among the sensitive population can give rise to a much more adaptive phenotype for high concentrations of Nilotinib.

- The radiosensitivity of both tumor subphenotypes are set to be the same. The effect of Nilotinib on radiosensitivity is negligibly small. We also ignore any possible mutations that confer resistance due to ionizing radiation.

We assume the following for the normal lymphopoietic cell line:

- Nilotinib does not effect the proliferation or death rates of the normal lymphoblast population. Literature shows, *in vitro*, that nilotinib has only mild suppressive effect on normal lymphoblast cell proliferation in long-term cultures [1].

- Normal cells will have no capability to mutate to a Nilotinib sensitive or resistant cell, given that either therapy is not likely to induce the specific BCR-ABL translocation mutation the tumor subpoputations express.

- The normal cell population is resource constrained. In the absence of the tumor subpopulations, the normal cells exist in healthy equilibrium as fully functional. Our model includes both a viability-dependent division rate and a viability-independent cell death term to achieve this equilibrium. Furthermore, the normal cells at baseline will have a proliferation rate less than that of the tumor cells, due to the absence of autodimerization of the BCR-ABL mutation.

- The radiosensitivity of the normal cells remains constant, both in the absence and presence of nilotinib. We ignore any other possible mutations due to ionizing radiation.

The mathematical model represents the dynamics of the three cell lines. We denote the viability, or cell population normalized by the starting population in a control experiment, of normal lymphoblast cells with x_N, Nilotinib sensitive tumor cells with x_S and Nilotinib resistant tumor cells with x_R. The division and death rates of each cell line are denoted r_i and d_i, respectively, with $i = N, S, R$ respective to subscripts indicated in the viabilities. The total population can reach a maximum viability indicated by K. We set a constant mutation rate ν, where Nilotinib sensitive cells can transform into resistant cells. We write the killing induced by ionizing radiation treatment separately. From the linear-quadratic formula (see Appendix) it can be written proportional to dose delivery rate dD/dt, where $D(t)$ is total dose delivered at time t.
The dynamics can be captured in the following system of ordinary differential equations (ODEs),

$$\begin{aligned}
\frac{dx_N}{dt} &= r_N x_N \left(1 - \frac{x_S + x_R + x_N}{K}\right) - d_N x_N - \frac{dD}{dt}(\alpha + 2\beta D(t))x_N \\
\frac{dx_S}{dt} &= r_S x_S \left(1 - \frac{x_S + x_R + x_N}{K}\right) - d_S x_S - \frac{dD}{dt}(\alpha + 2\beta D(t))x_S - \nu x_S \\
\frac{dx_R}{dt} &= r_R x_R \left(1 - \frac{x_S + x_R + x_N}{K}\right) - d_R x_R - \frac{dD}{dt}(\alpha + 2\beta D(t))x_R + \nu x_S.
\end{aligned} \tag{2.1}$$

As discussed in the text we have assumed that the radiosensitivity parameters α and β are the same and constant for both tumor phenotypes and constant for normal lymphblast cells. The radiosensitivities of both tumor phenotypes were determined in Chapter 1, and normal lymphoblast parameters of $\alpha = 1.5, \beta = 0.15$ were obtained from [3]. We assume both proliferation rates and death rates for the tumor subpopulations are affected by Nilotinib, wereas this is not the case for normal lymphblasts.
While the the system of ODEs in Eq. 2.1 depict a direct competition between tumor and normal lymphoblast cells, a more realistic option may be to separate the cell lines into their own subpoputation *dishes* to better simulate the normal bloodstream, where cell counts can rise two or more times the maximum levels considered normal. This system is found in Eq. 2.2.

$$\begin{aligned}
\frac{dx_N}{dt} &= r_N x_N \left(1 - \frac{x_N}{K}\right) - d_N x_N - \frac{dD}{dt}(\alpha + 2\beta D(t))x_N \\
\frac{dx_S}{dt} &= r_S x_S \left(1 - \frac{x_S + x_R}{K}\right) - d_S x_S - \frac{dD}{dt}(\alpha + 2\beta D(t))x_S - \nu x_S \\
\frac{dx_R}{dt} &= r_R x_R \left(1 - \frac{x_S + x_R}{K}\right) - d_R x_R - \frac{dD}{dt}(\alpha + 2\beta D(t))x_R + \nu x_S.
\end{aligned} \tag{2.2}$$

The simluations attempt to minimize tumor cell viability over a 10 day period, denoted f, while maximizing normal lymphoblast cell viability, denoted g. Using an optimization routine in MATLAB, the minimum of $f - g$ was found under the constraints to be discussed below on g. The total radiation per 5 day treatment protocol was limited to 2Gy. The efficacy of each treatment protocol was determined by extending simulations over a 20 day period.

2.3 Results

2.3.1 Verification of the equilibrium of normal lymphoblasts

The model, as it has expanded with the additional spatial constraint of normal lymphoblast cells, must adhere to an equilibrium for normal lymphoblasts *in vitro*. As the previous model contains tumor cells only and has been optimized for such set up based on empirical data, the given K, or maximum viability, will remain 4.82. Thus, as the death rate d_i and K will directly affect the equilibrium, it was determined that $r_N = 2, d_N = 1.625$ would be appropriate given the constraints above. Fig. 2.1 depicts this scenario, without radiation or Nilotinib, and without tumor cells present. This viability curve is consistent with the tumor cell control experiment *in vitro* performed previously. Note that these viabilities must not sum to 1, as frequencies would require. In the absence of treatment, when the two populations are, theoretically, placed in direct competition *in vitro*, you can see in Fig. 2.2 that both subpopulations are equally as viable in the steady state but do have a severe decrease from initial viability due to resource constraints. Parameters are unchanged, and initial conditions held that initial viabilites for normal lymphoblasts, Nilotinib sensitive and Nilotinib resistant cells were

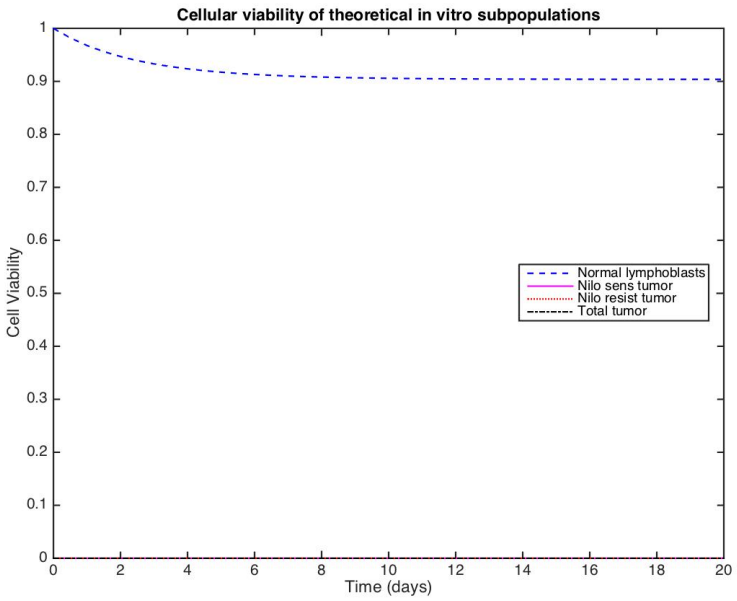

Figure 2.1: Normal cell equilibrium in the absence of treatment and tumor cells. Under spatial and resource constraints *in vitro*, the normal lymphoblast population has a steady state viability of around 90%.

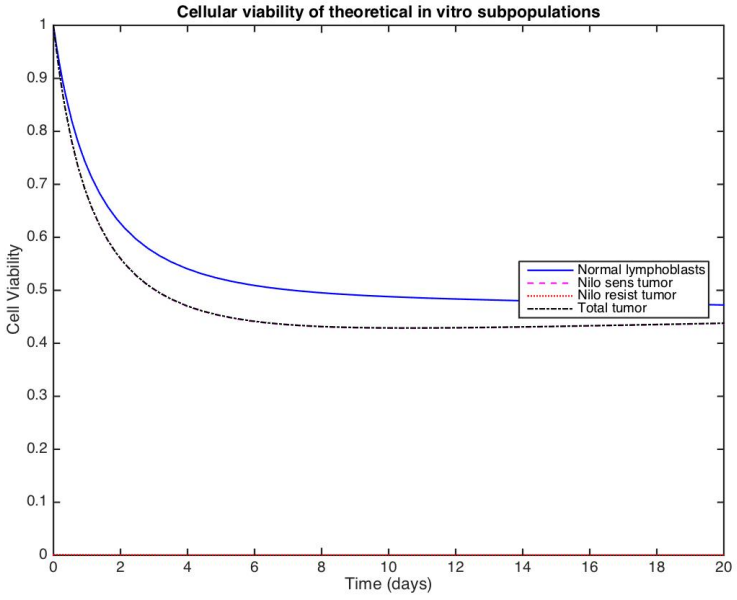

Figure 2.2: Interaction of cell supbpopulations in the absence of treatment. Direct competition with resource constraints indicate lower and nearly equally viable subpopulations. Note, however, the severely diminished populations ($<$50%).

$1, 1, 0.001$ respectively.

For comparison, Fig. 2.3 depicts the same simulation as in Fig. 2.2, however the subpopulations follow the new dynamics outlined in Eq. 2.2.

Note that in Fig. 2.3, each population, beginning at viability of 1, does decline in viability due to resource constraint amongst its respective subpopulation and are equally viable in the steady state. This appears to be most consistent with possible *in vivo* behavior as the circulatory system can maintain a significant population of lymphoblasts above normal, and our populations are derived with parameters set for a constrained system. Note that in Figs. 2.2 and 2.3 that there is a slow transformation of Nilotinib sensitive to resistant cells in the absence of Nilotinib. This is a consequence of optimimal parameterization fitting performed against the *in vitro* data in Chapter 1.

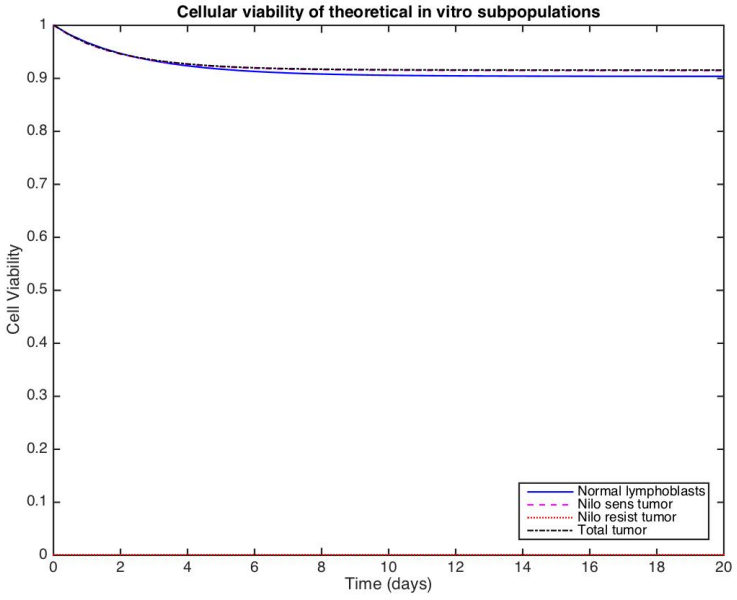

Figure 2.3: Subpopulations without treatment, with dynamics of *in vitro* growth separate between normal lymphoblast and tumor subpopulations. Note the slow transformation of Nilotinib sensitive to resistant cells while maintaining a steady state population equally viable to that of normal lymphoblasts.

2.3.2 Efficacy of previously proposed therapy strategies to minimize tumor burden

Our previous work was successful in modeling the *in vitro* behavior of ALL cells under various treatment protocols, allowing us to conclude that there is a synergistic effect conducting concurrent radiation and chemotherapies. We then suggested several optimized protocols in an attempt to minimize the tumor burden, both by optimizing radiation therapy protocols as well as altering Nilotinib dosing. Each of these protocols will be examined for their effect on normal lymphoblast cells to determine if such a protocol would be detrimental to a patient with a fully functional subpopulation of normal lymphoblast cells necessary for survival.

Four treatment protocols, as previously performed, will be simulated. First, 2Gy of acute radiation will be delivered at once, with constant 18 nM Nilotinib present throughout. Second, 5 fractions of 0.4Gy (2Gy total) radiation will be delivered at 1 day increments. Third, through a minimization protocol, it was determined that an optimal 5-fraction (delivered 1 day apart) would be: $d1 = 0.9371, d2 = 0.5139, d3 = 0.6445, d4 = 0.0450, d5 = 0.0064$ in the presence of constant 18 nM Nilotinib. Finally, the optimal radiation strategy is kept the same but the Nilotinib dosing is varied. The alternate Nilotinib delivery strategy maintains the average daily dose to be 18 nM, however begins at a lower concentration and increases throughout the therapy duration, given by three days of 10 nM, followed by four days of 18 nM, and finally three days of 26 nM Nilotinib. The Nilotinib dose returns to 18 nM for the duration of the simulation after that time.

2.3.2.1 Direct competition model under previous strategies

First we consider the direct competition dynamics where each subpopulation is interacting for resources. Figs. 2.4 and 2.5 depict each of the aforementioned strategies and their effects on the normal lymphoblast and tumor subpopulations. It is clear in each of the treatment strategies that the tumor populations are eradicated as the normal lymphoblast population returns to a higher steady state. The normal cell viability, however, does fall lower than 30% but returns to a higher steady state.

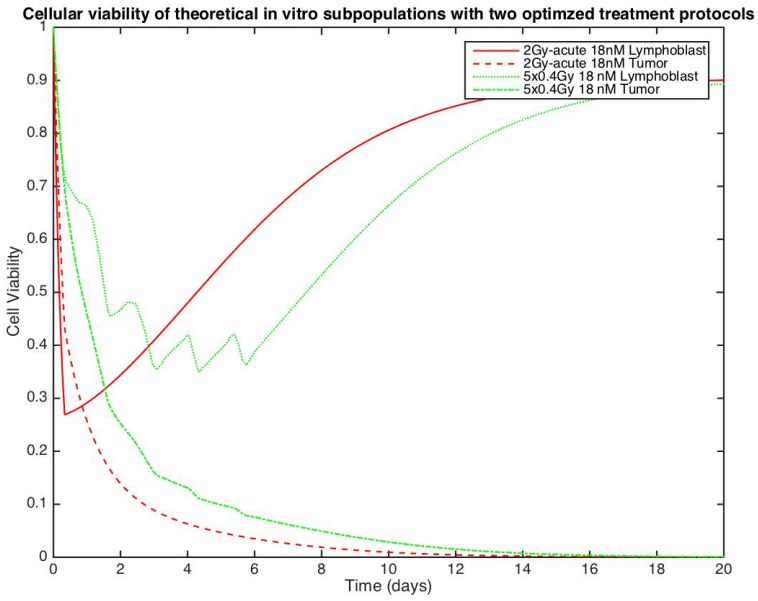

Figure 2.4: Effect of optimization protocols previously determined on competitive subpopulations. The 2Gy acute with 18 nM Nilotinib (red, solid and dashed) and 5x0.4Gy fractions with 18 nM (green, dotted and dashed-dotted) are depicted.

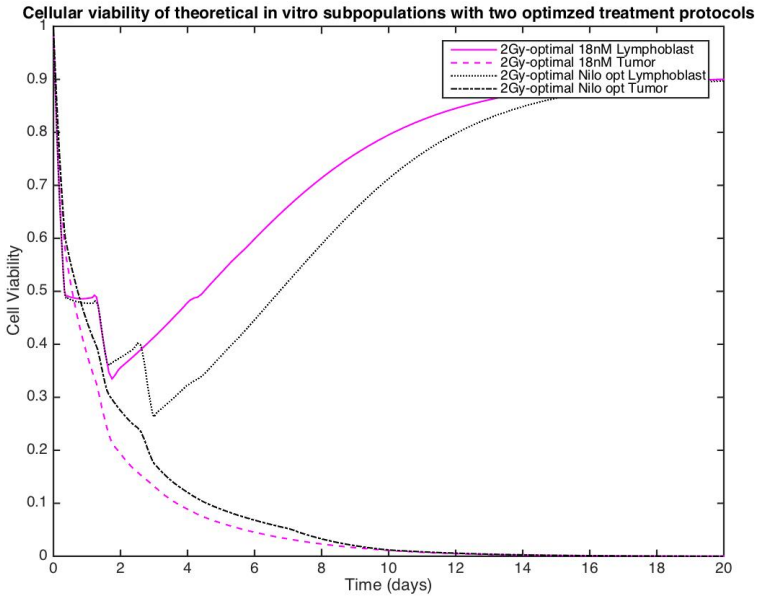

Figure 2.5: Effect of optimization protocols previously determined on competitive subpopulations. The 2Gy optimal radiation protocol with constant 18 nM Nilotinib (magenta, solid and dashed lines) and optimal 2Gy radiation protocol with back-loaded Nilotinib (black, dotted and dashed-dotted lines) are depicted.

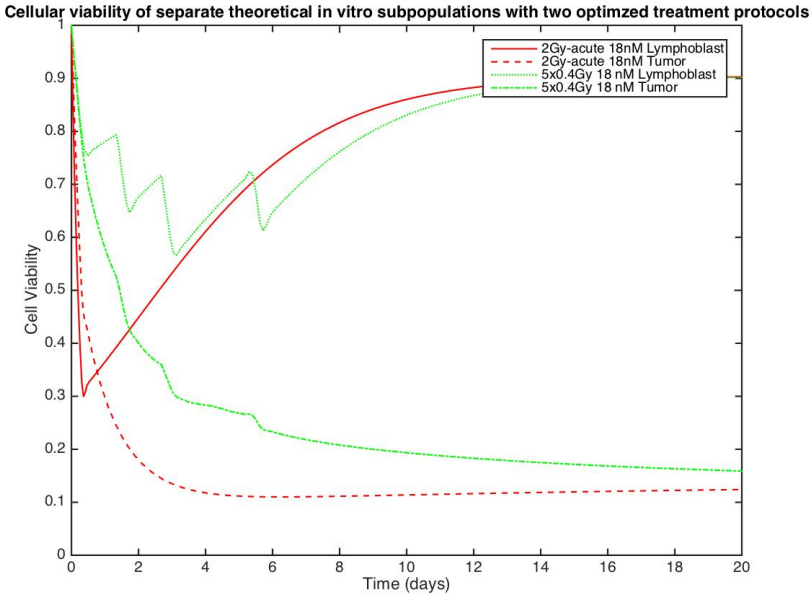

Figure 2.6: Effect of optimization protocols previously determined on separate subpopulations with separated subpopulations. The 2Gy acute with 18 nM Nilotinib (red, solid and dashed) and 5x0.4Gy fractions with 18 nM (green, dotted and dashed-dotted) are depicted.

2.3.2.2 Separate subpopulation model

Next we consider the ”separate” dynamics of the populations, where, in essence, the normal lymphoblast subpopulation and tumor subpopulations are considered separate and not in competition for resources in simulations. The four aformentioned protocols are depicted in Figs. 2.6 and 2.7. These simulations confirm the efficacy against the tumor populations previously shown, and the normal lymphoblast population returns to a healthy steady state much quicker than in the competetive model. The normal cell viabiliy, however, falls at most to 30% overall but does return to a higher steady state.

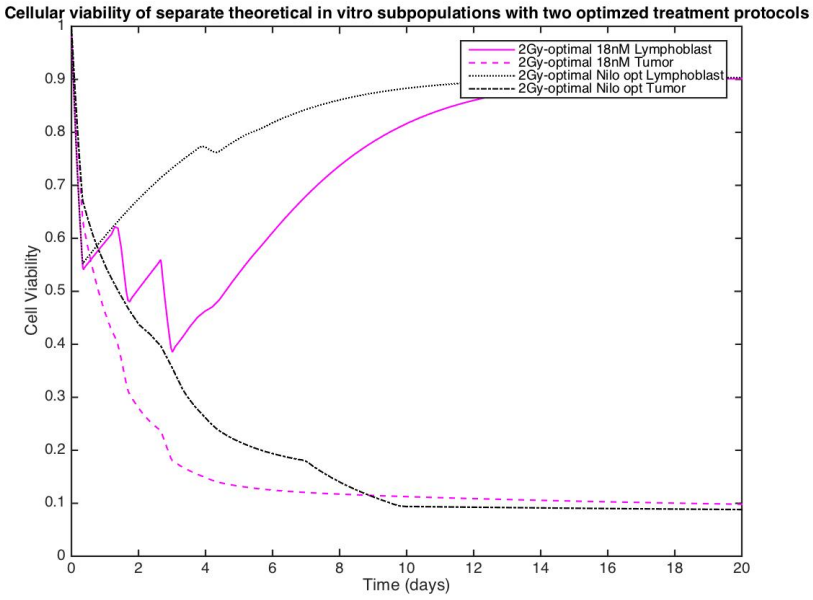

Figure 2.7: Effect of optimization protocols previously determined on separate subpopulations. The 2Gy optimal radiation protocol with constant 18 nM Nilotinib (magenta, solid and dashed lines) and optimal 2Gy radiation protocol with back-loaded Nilotinib (black, dotted and dashed-dotted lines) are depicted.

2.3.3 Proposed therapy strategies with normal lymphoblast cell toxicity constraint

The purpose of adding the normal lymphoblast cells to the model is to investigate the secondary effect that a therapy targeted toward tumor cell reduction might have on normal bodily function. In ALL, we are concerned with the fully functional lymphoblast population. Clinically, the white blood cell count (WBC) is used to assess the patient's status with leukocytosis (overabundance of white blood cells, *typically* found in infections) or leukocytopenia (too few white blood cells, making the patient more likely to become severely infected). We aim to avoid leukocytopenia. A patient with ALL will likely have leukocytosis by the WBC, where the majority of white blood cells are the tumorous, immature ALL cells. We assume, then, that there is some level of normal lymphoblasts in the patient. The WBC test has a range of acceptable values (for normal, functioning white blood cells), in thousands, of 4.5 to 11. We shall just average this to 7.75, and thus we can determine that the *average* acceptable percentage loss of normal cells is 41.9% to remain in a state that avoids immunosuppression. Of course, the ultimate goal is complete sparing of functional lymphoblasts but radiation does not allow this. Thus, the acceptable viability of normal lymphoblasts for the following simulations will not fall below 0.6. We will also consider thresholds of 0.75, 0.8, and 0.9 in the separate subpopulation model.

2.3.3.1 Direct competition model

The toxicity constraint of normal cell viability falling below 0.6 was first considered. Fig. 2.8 depicts this simulation, run with a constant concentration of 18 nM nilotinib throughout. The resultant optimal fractionation of radiation was as follows: $d1 = 1.2035, d2 = d3 = d4 = d5 = 0$. Simply, the radiation was front-loaded. Similarly, when the nilotinib was varied to be back-loaded (10 nM for 3 days, 18 nM for 4 days, 26 nM for 3 days in the treatment window and returning to 18 nM thereafter), as this was found optimal in Chapter 1, Fig. 2.9 shows radiation delivery fractions of $d1 = 1.0214, d2 = 0.023, d3 = 0.0254, d4 = 0, d5 = 0.0031$. This, again, essentially front-loads the radiation and disperses small doses for the remainder of the protocol. Note that the back-loaded nilotinib protocol requires less radiation overall for treatment.

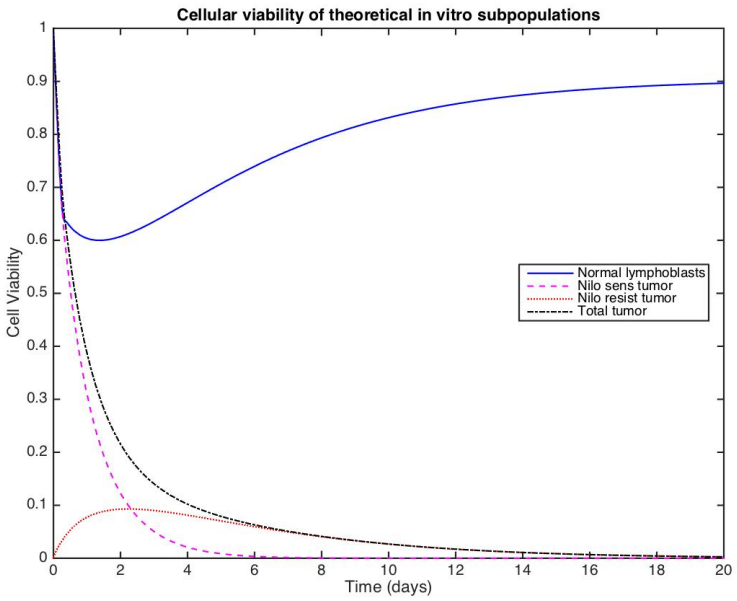

Figure 2.8: Direct competition simulation with normal lymphoblast toxicity constraint greater than 60%, with constant nilotinib (18 nM). The surviving normal lymphoblasts after irradiation dominate the culture and out-compete the tumor cells.

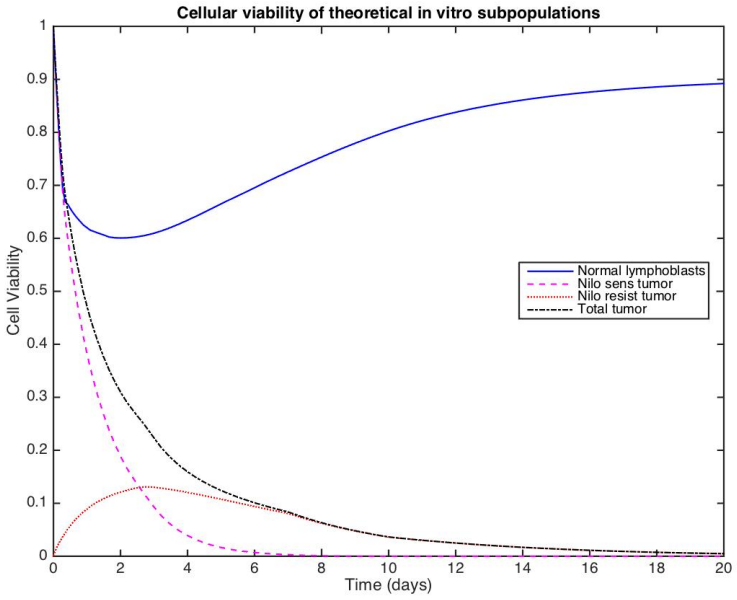

Figure 2.9: Direct competition simulation with normal lymphoblast toxicity constraint greater than 60%, with back-loaded nilotinib protocol. The surviving normal lymphoblasts after irradiation dominate the culture and out-compete the tumor cells, with less radiation required.

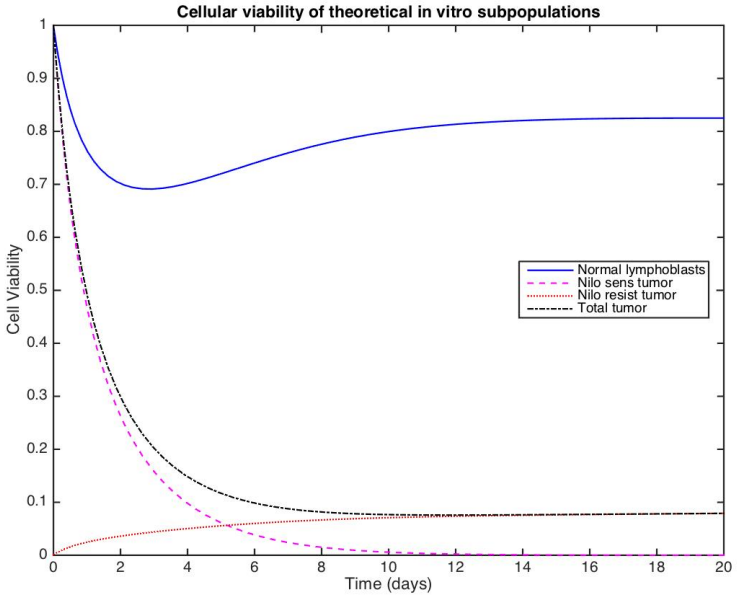

Figure 2.10: Direct competition simulation with nilotinib-only protocol, constant 18 nM. Note the drop in normal lymphoblast viability below 70% secondary to competition with tumor cells.

However, further optimizations requiring a higher viability using the direct competition model were futile, as depicted in Figs. 2.2 and 2.10. Fig. 2.10 shows radiation-free protocol with nilotinib only. Note the drop in viability secondary to the presence of tumor cells, though less severe than in Fig. 2.2 due to the death of tumor cells initially and establishment of a steady state greater than the tumor population. Therefore, further attempts with optimization of this model were not performed.

2.3.3.2 Separate subpopulation model

Considering the separate supopulations *in vitro* allows greater exploration into various allowable toxicity constraints. Each of constant 18 nM and back-loaded nilotinib protocols were used, and constraints of minimum allowable viablities of 60%, 75%, 80% and 90% were investigated. The radiation doses for each simulation are outlined in Table 2.1.

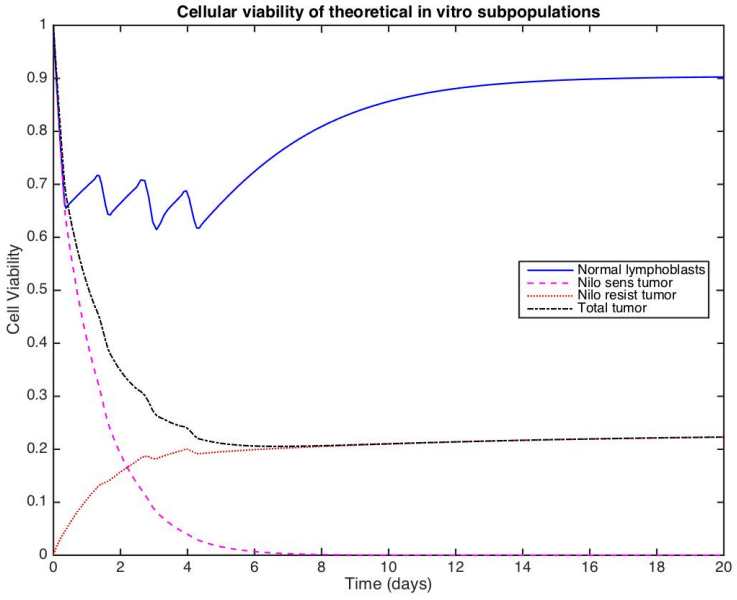

Figure 2.11: Separate subpopulation simulation with constant 18 nM nilotinib and minimum threshold of 60% normal lymphoblasts.

The 60% minimum constraint on normal lymphoblasts resulted in front loading radiation in the constant nilotinib simulation, and in more distributed fractions but still front-loaded for back-loaded nilotinib. Both protocols returned the normal lymphoblasts to steady state in the 10 day time frame but the back-loaded nilotinib suppressed the tumor population to a lower viability over time. After two days of therapy the resistant subpopulation emerges as the sole tumor population. These are depicted in Figs. 2.11 and 2.12.

A minimum normal lymphoblast viability of 75% results in front-loaded radiation fractions, but with small fractions spread out in the case of constant nilotinib (Fig. 2.13). In the back-loaded nillotinib case, the first two fractions are larger, while the remaining taper off (Fig. 2.14). The larger dose of radiation appears to allow better control of the tumor subpopulation in back-loaded nilotinib, while still allowing the return of the normal lymphoblast subpopulation to normal steady state. Fig. 2.14, the back-loaded nilotinib protocol, also appears to perform slightly better in the return of the tumor subpopulation than the constant nilotonib protocol. Note also the higher tumor viability (roughly 10%)

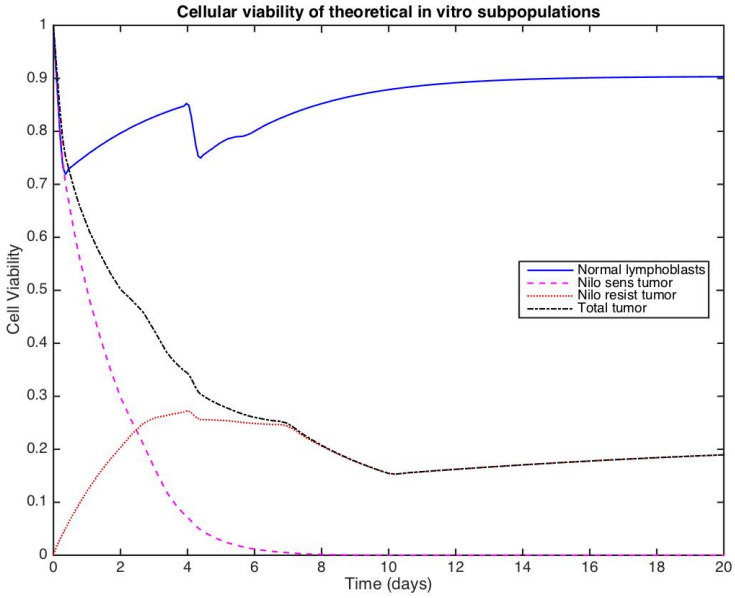

Figure 2.12: Separate subpopulation simulation with back-loaded nilotinib and minimum threshold of 60% normal lymphoblasts.

at the end of each similuation compared to Figs. 2.11 and 2.12. A resultant tumor population of resistant tumor cells again emerges in both.

Both nillotinib protocols in a toxicity constraint minimum of 80% normal lymphoblasts front-load the radiation, yet still disperse smaller fractions for the remainder of the protocol (Figs. 2.15 and 2.16). In these cases, the total radiation delivered at any time is very limited and the tumor population rebounds fairly well, to about 50%. This is much higher than the first two toxicity constraints (Figs. 2.11 - 2.14). In addition, the constant nilotinib protocol fares better in terms of tumor suppression over a longer period than the back-loaded nilotinib, but only slightly (within a few percentage points). Again is seen the development of the resistant tumor subpopulation in response to this therapy. Finally, limiting the viability of normal lymphoblasts to a minimum of 90% further limits the doses of radiation. In both nilotinib protocols, the fractions were front loaded but due to the diminished nature of the dosing size there are several equivalent doses that then taper off. In Figs. 2.17 and 2.18, note the sparing of the normal lymphoblasts essentially at steady state with the near full recovery of resistant tumor cells equally

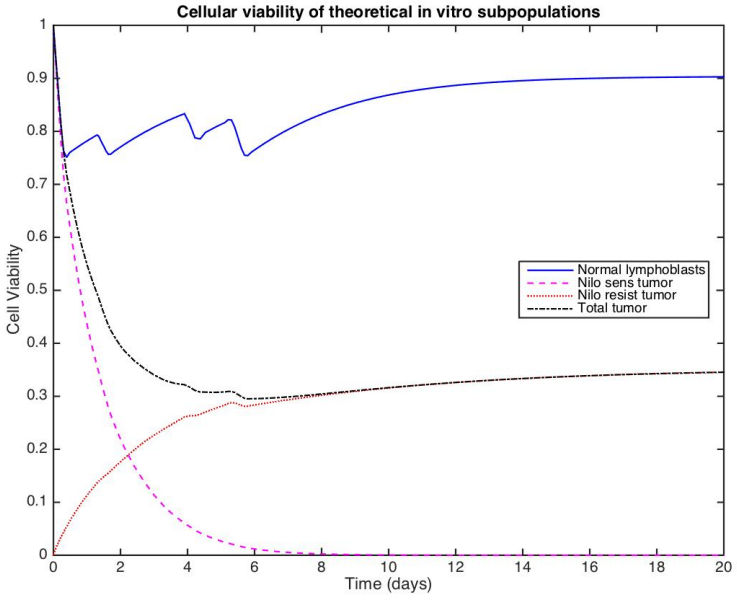

Figure 2.13: Separate subpopulation simulation with constant 18 nM nilotinib and minimum threshold of 75% normal lymphoblasts.

in both cases. The normal lymphoblasts survive and repopulate but due to their own spatial constraint *in vitro* they fall to a steady state of approximately 90%. Both therapy protocols result in tumor viabilty of approximately 63% after 20 days, comprised completely of the resistant subpopulation.

2.4 Discussion

The various simulations provide insight into the balance clinicians must make in treatment using radiation; that is, there is a trade-off to spare functional tissue in order to reduce tumor size. The direct competition model simulations illustrate the effects of an overabundance of tumor cells, seen in Fig. 2.2. However, this competition allows a better prognosis, that is, less tumor burden after treatment, in treatment protocol simulations as the normal lymphoblasts survive irradiation and establish at a higher fitness than tumor cells. In treatment cases, seen in Figs. 2.8 and 2.9, the tumor burden is

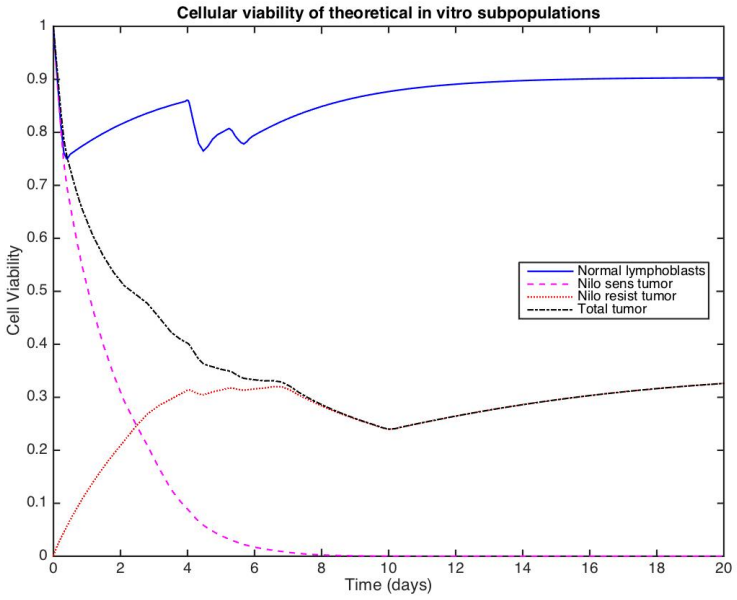

Figure 2.14: Separate subpopulation simulation with back-loaded nilotinib and minimum threshold of 75% normal lymphoblasts.

Table 2.1: Optimal Dosing Strategies. The doses below are the output protocols determined with the opimization routine. *Comp* refers to direct competition model, *sep* is the separate population model, *C* is constant 18 nM nilotinib and *BL* is back-loaded nilotinib protocol. Each percentage is the minimum viability threshold for the given protocol. $d1, d2, d3, d4, d5$ are radiation fractions, with Gy units.

	Comp 60%, C	Comp 60%, BL	Sep 60%, C	Sep 60%, BL	Sep 75%, C
d1	1.2035	1.0214	0.7762	0.6915	0.6894
d2	0	0.023	0.3192	0.4229	0.1526
d3	0	0.0254	0.3853	0.3811	0.2017
d4	0	0	0.2802	0.2823	0.2023
d5	0	0.0031	0	0.0213	0.2007
	Sep 75%, BL	Sep 80%, C	Sep 80%, BL	Sep 90%, C	Sep 90%, BL
d1	0.6783	0.5002	0.5018	0.25	0.2489
d2	0.2001	0.1177	0.1164	0.25	0.2486
d3	0.1816	0.1447	0.1441	0.1034	0.1024
d4	0.267	0.149	0.15	0.0841	0.0988
d5	0.1226	0.2	0.1454	0.0004	0.0077

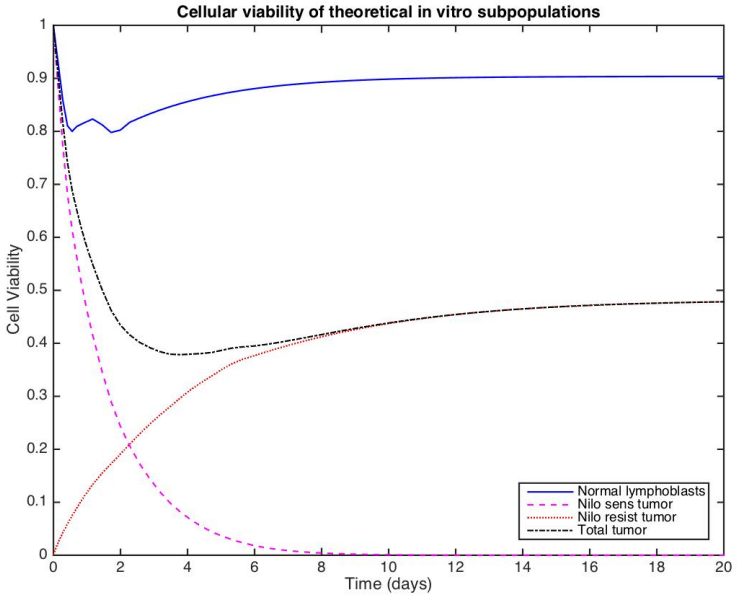

Figure 2.15: Separate subpopulation simulation with constant 18 nM nilotinib and minimum threshold of 80% normal lymphoblasts.

nearly eradicated by the end of a 20 day period due to this competition. The competition disallowed further investigation into sparing techniques due to the expected drop in viability. While this competition theoretically exists *in vivo*, it is a consequence of *in vitro* experiments that this arises. It is also important to note that this model required less radiation when using the back-loaded nilotinib protocol, indicating that the combination of therapies may potentially spare the patient of higher doses of common protocols. While the direct competition model for treatments *in vitro* is correct in theory, it is limited by the spatial constraints it is placed under by nature of the *in vitro* tumor subpopulation parameters found previously. Further, a patient's WBC as previously discussed can exceed two to three or more times a normal WBC.

The simulations utilizing separate subpopulations, essentially one petry dish for tumor cells and one for normal cells, are more realistic in determining the efficacy of treatment protocols if we wish to extend this model closer to *in vivo* situations. The treatment protocols for each 60%, 75%, 80% and 90% minimum thresholds (Figs. 2.11-2.18) depict the level to which a clinician may adjust treatment for a efficacious outcome given a

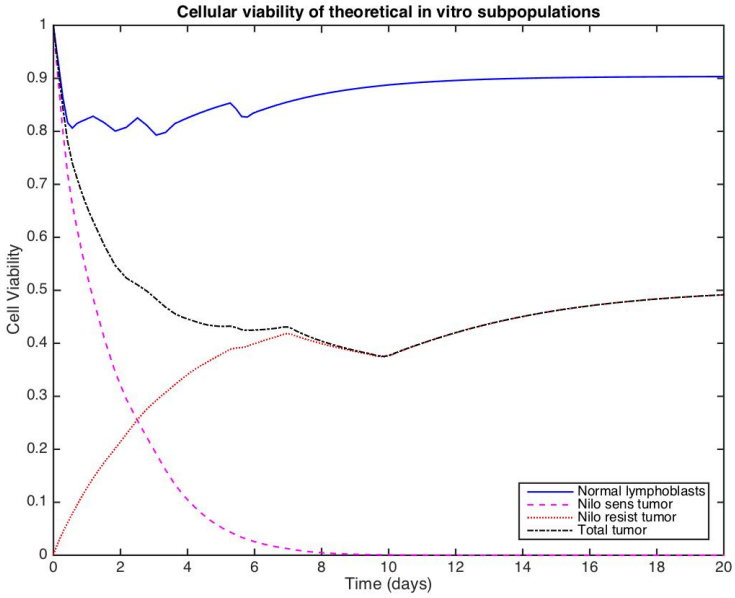

Figure 2.16: Separate subpopulation simulation with back-loaded nilotinib and minimum threshold of 80% normal lymphoblasts.

patient's particular status (as only a certain functional lymphoblast loss may be acceptable). Note, however, as the minimum threshold rises there is both an associated decrease in radiation as well as drop in efficacy of the treatment. Resistance to nilotinib clearly emerges in each simulation, and the radiation therapy provides the suppression of the resistant tumor cells. Thus removing and reducing doses of radiation inhibits the ability to control the tumor population resistant to nilotinib.

The previous protocols determined to control the tumor population were also evaluated. The direct competition model again saw the eradication of the tumor subpopulations, and very quickly, but with the consequence of nearly 75% loss of normal lymphoblasts (Figs. 2.4 and 2.5). This loss of functional tissue is too large for an acceptible clinical outcome. The separate subpopulation model matched the tumor subpopulation behavior of the previous results, but also depicting the effect on the normal lymphoblasts (Figs. 2.6 and 2.7). The loss of normal lymphoblasts ranged from 45-70%. Again, these treatment protocols border and exceed the acceptable limits of functional tissue loss caused by the treatment protocols.

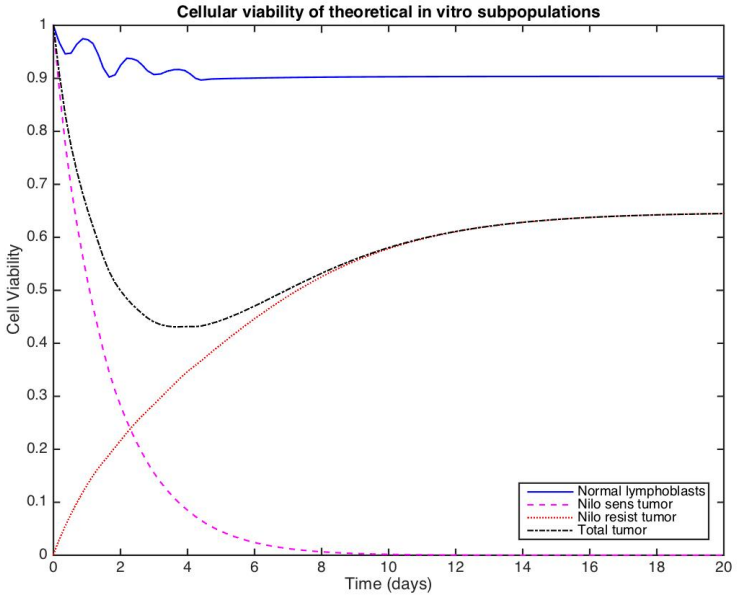

Figure 2.17: Separate subpopulation simulation with constant 18 nM nilotinib and minimum threshold of 90% normal lymphoblasts.

Investigation of the various radiation dosing strategies indicates that an initial, large acute dose of radiation followed by smaller doses coupled with nilotinib suppresses tumor viability overall. The suppression of the emerging resistant population is essential, and the smaller, subacute radiation doses provide this benefit along side the back-loaded nilotinib protocol. Thus, the fractionation of the radiation dose allows for a less aggressive treatment overall that compliments the suppression of the tumor cell population in the long term. The current modality of chemotherapy allows greater toxicity flexibility (of normal lymphoblastic cells) as nilotinib only greatly affects the Ph+ ALL cells.

The results indicate that there is both flexibility and individualization to concurrent therapies in the clinical setting. While this study is limited to parameters determined from *in vtiro* data, similar analyses from experiments performed *in vivo* would allow greater insight into the biological response to this theory of treatment. Further, this model allows greater flexibility in the individualistic treatment protocol for a patient in the clinic. A physician has the ability to assess the patient's current condition (tumor burden,

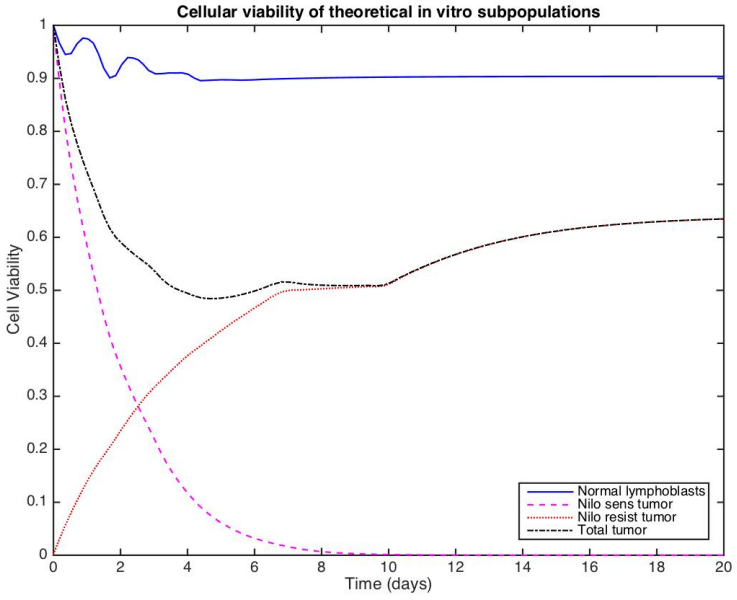

Figure 2.18: Separate subpopulation simulation with back-loaded nilotinib and minimum threshold of 90% normal lymphoblasts.

leukocytosis, tumor resistance, etc.) and apply a protocol that balances the goals of the therapy. While the radiation and nilotinib doses outlined above are not concrete in clinical implementation, they illustrate both the potential efficacy this specific combined therapy protocol may have as well as individualistic therapy options for physicians.

Chapter 3

References

[1] Ludovic Belle, France Bruck, Jacques Foguenne, André Gothot, Yves Beguin, Frédéric Baron, and Alexandra Briquet. Imatinib and nilotinib inhibit hematopoietic progenitor cell growth, but do not prevent adhesion, migration and engraftment of human cord blood cd34+ cells. *PLoS ONE*, 7(12):e52564, 2012.

[2] Niklas Feldhahn, Anna Arutyunyan, Sonia Stoddart, Bin Zhang, Sabine Schmidhuber, Sun-Ju Yi, Yong-mi Kim, John Groffen, and Nora Heisterkamp. Environment-mediated drug resistance in bcr/abl-positive acute lymphoblastic leukemia. *Oncoimmunology*, 1(5):618–629, 2012.

[3] Aiden A Flynn, Alan J Green, R Barbara Pedley, Geoffrey M Boxer, Jason Dearling, Rebecca Watson, Robert Boden, and Richard H J Begent. A model-based approach to the optimization or radioimmunotherapy through antibody design and radionuclide selection. *Cancer*, 94(4):1249–57, 2002.

[4] FX Gruber, T Ernst, K Porkka, RA Engh, I Mikkola, J Maier, T Lange, and A Hochhaus. Dynamics of the emergence of dasatinib and nilotinib resistance in imatinib-resistant cml patients. *Leukemia*, 26(1):172–177, 2012.

[5] Eric J Hall and Amato J Giaccia. *Radiobiology for the Radiologist*. Lippincott Williams & Wilkins, 2006.

[6] Hagop Kantarjian, Francis Giles, Lydia Wunderle, Kapil Bhalla, Susan O'Brien,

Barbara Wassmann, Chiaki Tanaka, Paul Manley, Patricia Rae, William Mietlowski, et al. Nilotinib in imatinib-resistant cml and philadelphia chromosome–positive all. *New England Journal of Medicine*, 354(24):2542–2551, 2006.

[7] Pavinder Kaur, Niklas Feldhahn, Bin Zhang, Daniel Trageser, Markus Muschen, Veerle Pertz, John Groffen, and Nora Heisterkamp. Nilotinib treatment in mouse models of p190 bcr/abl lymphoblastic leukemia. *Mol Cancer*, 6(10):67, 2007.

[8] Dae-Young Kim, Young-Don Joo, Sung-Nam Lim, Sung-Doo Kim, Jung-Hee Lee, Je-Hwan Lee, Dong Hwan Dennis Kim, Kihyun Kim, Chul Won Jung, Inho Kim, et al. Nilotinib combined with multiagent chemotherapy for newly diagnosed philadelphia-positive acute lymphoblastic leukemia. *Blood*, 126(6):746–756, 2015.

[9] Oliver G Ottmann and Heike Pfeifer. Management of philadelphia chromosome–positive acute lymphoblastic leukemia (ph+ all). *ASH Education Program Book*, 2009(1):371–381, 2009.

[10] Pier Paolo Piccaluga, Stefania Paolini, and Giovanni Martinelli. Tyrosine kinase inhibitors for the treatment of philadelphia chromosome-positive adult acute lymphoblastic leukemia. *Cancer*, 110(6):1178–1186, 2007.

[11] Uwe Rix, Oliver Hantschel, Gerhard Dürnberger, Lily L Remsing Rix, Melanie Planyavsky, Nora V Fernbach, Ines Kaupe, Keiryn L Bennett, Peter Valent, Jacques Colinge, et al. Chemical proteomic profiles of the bcr-abl inhibitors imatinib, nilotinib, and dasatinib reveal novel kinase and nonkinase targets. *Blood*, 110(12):4055–4063, 2007.

[12] Avichai Shimoni, Yulia Volchek, Maya Koren-Michowitz, Nira Varda-Bloom, Raz Somech, Noga Shem-Tov, Ronit Yerushalmi, and Arnon Nagler. Phase 1/2 study of nilotinib prophylaxis after allogeneic stem cell transplantation in patients with advanced chronic myeloid leukemia or philadelphia chromosome–positive acute lymphoblastic leukemia. *Cancer*, 121(6):863–871, 2015.

[13] Ke Yang and Li-wu Fu. Mechanisms of resistance to bcr–abl tkis and the therapeutic strategies: A review. *Critical reviews in oncology/hematology*, 93(3):277–292, 2015.

Appendices

A.1 Mutation-proliferation model

In this Appendix we present a simple model of mutation-proliferation that describes the dynamics of sensitive and resistant populations in the system. We denote the frequency of sensitive cells with x_{S} and resistants with x_{R}. Also, the division rate of sensitive cells are denoted by r_{S} and death rate with d_{S}. Similarly, the resistant phenotype divides and dies with rates r_{R} and d_{R}. The total population can reach a maximum viability indicated by K. We assume a constant mutation or transformation rate, ν, where sensitive cells can transform into resistant cells. We write the killing induced by radiation treatment separately. From the linear-quadratic formula (Appendix A.2) it can be written proportional to dose delivery rate dD/dt, where $D(t)$ is total dose delivered at time t. A schematic of possible proliferation and death events are depicted in Fig. 1. This dynamics can be captured in the following system of ordinary differential equations (ODE),

$$\begin{aligned}
\frac{\mathrm{d}x_{\mathrm{S}}}{\mathrm{d}t} &= r_{\mathrm{S}}x_{\mathrm{S}}\Big(1-\frac{x_{\mathrm{S}}+x_{\mathrm{R}}}{K}\Big)-d_{\mathrm{S}}x_{\mathrm{S}}-\frac{\mathrm{d}D}{\mathrm{d}t}\big(\alpha+2\beta D(t)\big)x_{\mathrm{S}}-\nu x_{\mathrm{S}},\\
\frac{\mathrm{d}x_{\mathrm{S}}}{\mathrm{d}t} &= r_{\mathrm{R}}x_{\mathrm{R}}\Big(1-\frac{x_{\mathrm{S}}+x_{\mathrm{R}}}{K}\Big)-d_{\mathrm{R}}x_{\mathrm{S}}-\frac{\mathrm{d}D}{\mathrm{d}t}\big(\alpha+2\beta D(t)\big)x_{\mathrm{R}}+\nu x_{\mathrm{S}}.
\end{aligned} \tag{1}$$

As discussed in the text we have assumed that radio-sensitivity parameters α and β are the same for both phenotypes. We assume both proliferation rates and death rates are affected by Nilotinib concentration. As discussed in the main text we use a linear regression dose response function given by Eq.1.2.

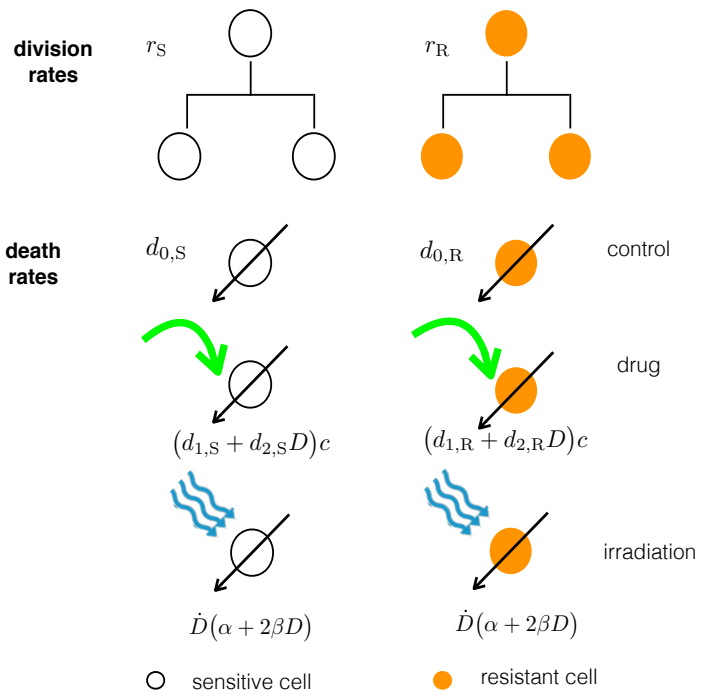

Figure 1: A schematic of possible proliferation and death events and corresponding rates in our model. For brevity the effect of Nilotinib and radiation on death rates are shown. In principle Nilotinib affects division/proliferation rates as well.

As discussed in the text, for control group the transformation rate, ν, is zero and proliferation and death rates of both populations are assumed to be equal. In this case the solutions of the proliferation-mutation model are straightforward. Denoting total frequency of cells by $x(t)$ and initial cell viability as $x_0 = \exp(-\alpha D - \beta D^2)$ we have

$$x(t) = \frac{e^{-\alpha D - \beta D^2} e^{(r-d)t}(r-d)}{e^{-\alpha D - \beta D^2}(e^{(r-d)t} - 1)r + r - d} \tag{2}$$

In fact we can use the above results to analytically approximate the values of radio-sensistivity coefficients. (See next Appendix.)

A.2 Continuous-time linear-quadratic formula

Effect of ionizing radiation on malignant/or normal cells is two fold. Single-strand or double-strand breaks of DNA causes some of the cells to undergo apoptosis. With a much smaller probability, ionizing radiation can cause mutations. In the following we ignore the mutation mechanism. The survival fraction, S, of cells that have been exposed to a radiation dose of D can be expressed by linear-quadratic formula,

$$S = e^{-\alpha D - \beta D^2}, \tag{3}$$

where α and β are radio-sensitivity parameters. We can express this in a continuous time format as well. In the absence of the cell proliferations we write the dynamics of total population as

$$\frac{\mathrm{d}x}{\mathrm{d}t} = -x(t)\big(\alpha + 2\beta D(t)\big)\frac{\mathrm{d}D}{\mathrm{d}t} \tag{4}$$

We can change variable from time t to dose delivered until time t, $D(t)$. The solutions for $x(t)$ as a function of dose are,

$$x(t) = x_0 e^{-\alpha D(t) - \beta D^2(t)} \tag{5}$$

where x_0 is the population before treatment. The survival fraction $x(t)/x_0$ is the thus given by well-known linear-quadratic formulae.

We can use the numerical values of the survival fraction in the in vitro experiments to

estimate the radio-sensitivity coefficients α and β. If the cell viabilities are measured right after for two separate administration values of radiation doses D_1 and D_2 we have

$$\begin{aligned} -\ln(S_1) &= \alpha D_1 + \beta D_1^2 \\ -\ln(S_2) &= \alpha D_2 + \beta D_2^2 \end{aligned} \tag{6}$$

which gives

$$\begin{aligned} \alpha &= \frac{D_2^2 \ln S_1 - D_1^2 \ln S_2}{D_2 D_1^2 - D_1 D_2^2} \\ \beta &= \frac{D_2 \ln S_1 - D_1 \ln S_2}{D_2 D_1^2 - D_1 D_2^2} \end{aligned} \tag{7}$$

If the cell viabilities are measured after time t, this gives time for a partial repopulation of the cells, and thus we need to take repopulation dynamics into account. Denoting death and birth rates as r and d and S_1, S_2 as cell viabilities measured at time t after irradiation then radio-sensitivities are

$$\begin{aligned} \alpha &= \frac{D_2^2 \ln\Big(\frac{S_1(d-r)}{(S_1-1)r+d)e^{-(d-r)t} - S_1 r}\Big) - D_1^2 \ln\Big(\frac{S_2(d-r)}{(S_2-1)r+d)e^{-(d-r)t} - S_2 r}\Big)}{D_1 D_2 (D_1 - D_2)} \\ \beta &= \frac{-D_2 \ln\Big(\frac{S_1(d-r)}{(S_1-1)r+d)e^{-(d-r)t} - S_1 r}\Big) + D_1 \ln\Big(\frac{S_2(d-r)}{(S_2-1)r+d)e^{-(d-r)t} - S_2 r}\Big)}{D_1 D_2 (D_1 - D_2)} \end{aligned} \tag{8}$$